



doi:10.1016/S0016-7037(03)00174-1

Isotope fractionation by chemical diffusion between molten basalt and rhyolite

FRANK M. RICHTER,¹ ANDREW M. DAVIS,^{1,2,*} DONALD J. DEPAOLO,³ and E. BRUCE WATSON⁴¹Department of the Geophysical Sciences, The University of Chicago, 5734 South Ellis Avenue, Chicago, IL 60637, USA²Enrico Fermi Institute, The University of Chicago, 5640 South Ellis Avenue, Chicago, IL 60637, USA³Department of Earth and Planetary Sciences, University of California, Berkeley, CA 94720, USA⁴Department of Earth & Environmental Sciences, Rensselaer Polytechnic Institute, Troy, NY 12180, USA

(Received August 15, 2002; accepted in revised form February 27, 2003)

Abstract—Experimental diffusion couples were used to study chemical diffusion between molten rhyolite and basalt with special emphasis on the associated fractionation of calcium and lithium isotopes. Diffusion couples were made by juxtaposing firmly packed powders of a natural basalt (SUNY MORB) and a natural rhyolite (Lake County Obsidian) and then annealing them in a piston cylinder apparatus for times ranging from 0.1 to 15.7 h, temperatures of 1350–1450°C, and pressures of 1.2–1.3 GPa. Profiles of the major elements and many trace elements were measured on the recovered quenched glasses. The diffusivities of all elements except lithium were found to be remarkably similar, while the diffusivity of lithium was two to three orders of magnitude larger than that of any of the other elements measured. Chemical diffusion of calcium from molten basalt into rhyolite was driven by a concentration ratio of ~ 18 and produced a fractionation of ^{44}Ca from ^{40}Ca of about 6%. Because of the relatively low concentration of lithium in the natural starting materials a small amount of spodumene ($\text{LiAlSi}_2\text{O}_6$) was added to the basalt in order to increase the concentration difference between basalt and rhyolite, which was expected to increase the magnitude of diffusive isotopic fractionation of lithium. The concentration ratio between Li-doped basalt and natural rhyolite was ~ 15 and the resulting diffusion of lithium into the rhyolite fractionated ^7Li from ^6Li by about 40%. We anticipate that several other major rock-forming elements such as magnesium, iron and potassium will also exhibit similarly larger isotopic fractionation whenever they diffuse between natural melts with sufficiently large differences in the abundance of these elements. Copyright © 2003 Elsevier Ltd

1. INTRODUCTION

Natural processes can alter the isotopic composition of geologic materials in a number of different ways, and in favorable circumstances, the resulting fractionations can be used to document the conditions and particular processes that operated. An extensively studied and well-understood case is that of equilibrium isotope fractionation due to differences in the zero point energy of molecules of different isotopic composition (Urey, 1947). The distribution of isotopes between coexisting phases reflects differences in chemical activity, which can be expressed in terms of partition functions $Q = \sum g_i e^{-E_i/kT}$, where the sum is taken over all energy levels E_i with weights g_i ; k is the Boltzmann constant, and T is absolute temperature. Mass-dependent isotopic fractionations arise because the energy levels E_i depend on mass. The partition functions also depend on temperature, which is what makes equilibrium isotopic fractionations so widely used as thermometers. The dependence on temperature is such that equilibrium isotope fractionations are greatest at low temperatures and become vanishingly small at high temperatures where isotopic partition functions tend to unity. Isotope fractionation will also take place during unidirectional reactions whenever reaction rates are different for different isotopes. This is often referred to as chemical kinetic isotope fractionation and it has been extensively documented and studied because it is commonly associated with vital processes in biologic systems. A classic example is the fractionation of carbon isotopes during photosynthesis (Park and Epstein, 1960).

Another type of isotopic fractionation is what we will refer to as physical kinetic fractionation. Under this heading we include isotope fractionations due to mass transport processes within a phase (e.g., diffusion) or between phases (e.g., evaporation). A well-known example of the former is the separation of isotopes by diffusion in a gas. The kinetic theory of nonuniform gases (see Chapman and Cowling, 1952) shows that in the case of a monatomic gas the ratio of the diffusivity of two isotopes of mass m_1 and m_2 is given by $D_1/D_2 = \sqrt{m_2/m_1}$. In the more common situation of dilute, isotopically distinct, species of mass m_1 and m_2 (e.g., H_2O and HDO vapor) diffusing through a gas of molecular weight M (e.g., air), the kinetic theory result is that the ratio of the diffusivities is $D_1/D_2 = \sqrt{m_2(m_1 + M)/m_1(m_2 + M)}$. Kinetic isotope fractionations by evaporation are also well known for liquids ranging from water (e.g., Craig et al., 1963) to molten silicates (e.g., Davis et al., 1990). A distinctive and very important attribute of the physical kinetic isotope fractionations is that they are independent of temperature and thus can occur and document events at high temperature where the equilibrium fractionations will have become negligible.

Richter et al. (1999) used laboratory experiments to show that significant kinetic isotopic fractionations can also occur during diffusion in molten oxides. These experiments involved diffusion couples of isotopically doped materials that were specifically designed to determine the relative mobility (i.e., the self-diffusion coefficients) of ^{76}Ge vs. ^{70}Ge in molten GeO_2 and ^{48}Ca vs. ^{40}Ca in a $\text{CaO-SiO}_2\text{-Al}_2\text{O}_3$ melt. Germanium was used as an analog for silicon to take advantage of the much lower melting point of GeO_2 compared to that of SiO_2 . The results showed no measurable fractionation of the germanium isotopes by diffusion. However, in the case of calcium isotopes

* Author to whom correspondence should be addressed (adavis@uchicago.edu).

diffusing in a CaO-Al₂O₃-SiO₂ melt, there was clear evidence of ⁴⁰Ca having distinctly greater mobility than ⁴⁸Ca. Richter et al. (1999) summarized the mass dependence of the self-diffusion coefficients of the isotopes of germanium and calcium in terms of a relationship of the form $D_1/D_2 = (m_2/m_1)^\beta$, with $\beta < 0.025$ for germanium isotopes and $\beta = 0.05\text{--}0.1$ for calcium isotopes. That germanium isotopes are not measurably fractionated by diffusion in molten GeO₂ was not surprising given that germanium and silicon are expected to behave in much the same way and molecular dynamics calculations by Zhou (1997) had already suggested that there should be no mass dependence of the mobility of silicon isotopes in molten SiO₂. The isotopic fractionation of calcium isotopes during diffusion in molten oxides could also have been anticipated, assuming that magnesium is an analog for calcium and given that molecular dynamics calculations of Tsuchiyama et al. (1994) show a mass dependence of magnesium isotopes diffusing in molten MgO corresponding to $\beta = 0.0969$. It should be kept in mind that the molecular dynamics calculations for molten oxides involve relatively small systems (~1000 particles), very short time scales (picoseconds), and extreme conditions (T~4000K). Laboratory experiments remain the most direct way of demonstrating and characterizing kinetic isotope fractionations associated with mass transport processes.

Richter et al. (1999) discussed (and summarized in their Fig. 8) what they believed to be the likely magnitude of isotopic fractionations by diffusion between natural melts. They pointed out that the degree of isotopic fractionation during chemical diffusion will depend not only on the relative mobility of the isotopes (i.e., β) but also on the concentration contrast between the interdiffusing melts. The dependence on the concentration contrast is due to the flux of the isotopically fractionated material being, to a good approximation, proportional to the elemental concentration difference and its effect will be greatest in the region with low concentration. The concentration contrast of Si and O between natural silicate melts is never very large (i.e., less than a factor of two) thus the isotopes of silicon and oxygen are not expected to be measurably fractionated by chemical diffusion in natural settings. Diffusion of calcium and magnesium, on the other hand, was predicted to fractionate ⁴⁴Ca/⁴⁰Ca and ²⁶Mg/²⁴Mg by as much as 10%, given typical concentration ratios of about a factor of 10 for these elements between rhyolitic and basaltic melts. It was also suggested that lithium isotopes might be even more significantly fractionated, by perhaps as much as several tens of %.

There are numerous reasons why the potential for isotopic fractionation by diffusion in silicate melts needs to be further documented by laboratory experiment. In terms of prior work, the most obvious is that Richter et al. (1999) measured the relative mobility of isotopes only in isochemical systems. It is well known that species having very different mobility (i.e., self-diffusion coefficients) when measured in an isochemical system can have very similar effective diffusivity during chemical diffusion (see Liang et al., 1996a, 1996b, 1997 for recent experiments and theoretical considerations bearing on self-diffusion vs. chemical diffusion). This raises the possibility that the relative mobility of the isotopes will not be fully reflected in their transport behavior during chemical diffusion. Another reason is to extend the earlier results to additional isotopic systems. In the case of lithium, Richter et al. (1999) did not

actually measure lithium isotope fractionations, thus their suggestion that lithium isotopes might be very significantly fractionated by diffusion between silicate melts needs to be verified and quantified by appropriate experiments. Clearly, the most direct way of showing that chemical diffusion between natural silicate melts can produce significant isotopic fractionations is to measure these fractionations in diffusion couples made from natural materials.

In this paper we report on new laboratory experiments involving diffusion couples made from molten natural materials (obsidian and midocean ridge basalt) that show large isotopic fractionations (relative to analytical precision) of ⁴⁴Ca from ⁴⁰Ca, and ⁷Li from ⁶Li. The results confirm that given a sufficiently large concentration contrast, chemical diffusion between natural melts will be marked by measurable isotopic fractionation. An unanticipated result was finding that lithium diffuses between molten basalt and molten rhyolite at an extraordinarily fast rate. The effective diffusivities of all the major elements, and 15 trace elements besides lithium, were found to be very similar (i.e., within a factor of about two). Lithium, depending on melt composition, was found to have an effective diffusivity a factor of 100 to 1000 times larger than that of all the other elements we measured. The only species that we are aware of that have similarly large diffusivities to that of lithium in molten silicates are dissolved molecular H₂O and helium.

2. EXPERIMENTAL AND ANALYTICAL METHODS

Diffusion couples were constructed by juxtaposing firmly packed powders made from natural basalt (SUNY MORB) and a natural rhyolite (Lake County Obsidian) in graphite capsules. The major element composition of the basalt and the obsidian used in the experiments are given in Table 1. Also listed in Table 1 are the composition of a series of intermediate-composition glasses that were made by melting mixtures with different proportions of basalt and rhyolite. These glasses were used to determine matrix effects due to major element composition on ion microprobe measurements of trace element concentrations and lithium isotopic composition. Figure 1a shows a schematic diagram of the graphite capsule that is part of the piston cylinder assembly used to anneal the diffusion couples at temperatures of 1350–1450°C and pressures of 1.2–1.3 GPa. The experiments were run at elevated pressures to avoid formation of bubbles, which can generate unwanted motions as they migrate upward due to buoyancy. The piston-cylinder apparatus was chosen for its high-temperature and rapid-quench capabilities. The experiments were run at 1.2 or 1.3 GPa (see Table 2) in 19-mm diameter assemblies consisting of NaCl and Pyrex™ outer sleeves with MgO filler pieces inside a tubular graphite furnace (see Fig. 1a). The samples were cold-pressurized to a value 10–20% above the desired run pressure, then heated at rates ranging from 75° to 270°C min⁻¹ (see Table 2). Final pressure adjustments were made following relaxation of the assembly as it approached run temperature. Figure 1a shows the positioning and approximate precompaction dimensions of the graphite-encapsulated basalt/obsidian interdiffusion couples, as well as the estimated axial temperature distribution as determined for nearly identical assemblies by Watson et al. (2002). Experiments were terminated by cutting power to the furnace, which resulted in cooling to below ~300°C in 20–30 s.

Figure 1b is a backscattered-electron image of an axis-parallel section of RB-2, obtained by grinding through the graphite container and a portion of the quenched diffusion couple. As is typical of piston-cylinder run products, numerous decompression cracks are evident, however as will be seen below, these do not significantly distort the measured diffusion profiles.

Profiles of major element concentration were measured along the length of the diffusion couples listed in Table 2 using a JEOL JSM-5800LV scanning electron microscope equipped with an Ox-

Table 1. Major element composition, in oxide wt.% unless otherwise indicated, of starting materials and mixed glass compositions.

	Starting compositions							
	Obsidian			SUNY MORB			Li-MORB	
	WDS ¹	IMP ²	EDS ³	WC ⁴	IMP ²	EDS ³	IMP ²	EDS ³
Li (ppm)		51.9			9.37		783	
Na ₂ O	4.31	4.69	4.38 ± 0.05	2.89	2.62	3.08 ± 0.05	2.35	2.98
MgO	0.07	0.09	0.12 ± 0.02	8.56	9.00	8.51 ± 0.06	8.86	8.25
Al ₂ O ₃	13.35	12.17	13.11 ± 0.07	16.07	16.19	15.83 ± 0.07	16.65	16.03
SiO ₂	76.37	≅75.93	75.93 ± 0.13	49.75	≅50.20	50.20 ± 0.13	≅50.49	50.49
K ₂ O	4.67	5.41	4.93 ± 0.05	0.18	0.22	0.22 ± 0.02	0.17	0.18
CaO	0.51	0.65	0.58 ± 0.04	10.80	11.05	10.91 ± 0.08	10.86	10.80
TiO ₂	0.15	0.12	0.12 ± 0.05	1.63	1.62	1.59 ± 0.05	1.64	1.56
MnO		0.08	0.08 ± 0.05		0.15	0.22 ± 0.05	0.15	0.21
FeO	0.79	0.76	0.76 ± 0.06	9.49	8.79	9.44 ± 0.12	8.51	9.52

	Intermediate composition standards						
	OB-1 ³	OB-2 ³	OB-3 ³	OB-4 ³	OB-5 ³	OB-6 ³	OB-7 ³
Na ₂ O	4.27	4.05	3.92	3.77	3.61	3.41	3.24
MgO	1.13	2.17	3.30	4.29	5.29	6.36	7.48
Al ₂ O ₃	13.43	13.78	14.08	14.42	14.81	15.13	15.44
SiO ₂	72.75	69.52	66.21	63.02	59.88	56.72	53.21
K ₂ O	4.39	3.83	3.14	2.57	2.01	1.42	0.76
CaO	1.83	3.16	4.53	5.79	7.04	8.33	9.68
TiO ₂	0.30	0.47	0.65	0.84	1.00	1.17	1.38
MnO	0.10	0.12	0.13	0.13	0.18	0.13	0.18
FeO	1.80	2.91	4.04	5.18	6.20	7.34	8.63

¹RPI electron probe.²Chicago ion microprobe.³Chicago SEM, given with 1σ standard deviations typically obtained for run product profiles.⁴Wet chemical analyses of bulk rock (personal communication, F. Shido, SUNY Albany).

ford Link ISIS-300 energy dispersive X-ray microanalysis system (EDS). The microanalysis system is capable of operating at total count rates of up to 50000 counts per second, which in the SEM can be achieved with a 15 kV primary beam current of 8 nA. Under these conditions precisions of better than 1 relative% can be achieved. Typical precisions for basaltic and rhyolitic compositions are given in Table 1. The electron beam was rastered over a 10 μm square for each spot to avoid volatilization of sodium and potassium.

Trace element profiles and lithium isotopic compositions were measured using the modified AEI IM-20 ion microprobe at the University of Chicago. Lithium isotopic compositions are reported as δ⁷Li values, defined as

$$\delta^7\text{Li} = \left[\frac{(^7\text{Li}/^6\text{Li})_{\text{sample}}}{(^7\text{Li}/^6\text{Li})_{\text{standard}}} - 1 \right] \times 1000.$$

Trace elements were analyzed using methods described in Hinton et al. (1988), Davis et al. (1991), Simon et al. (1991), and MacPherson and Davis (1994). Calcium-normalized ion yields were assumed to be the same for all matrices and were taken from averages of a variety of standard minerals and glasses. It has previously been observed that the calcium-normalized ion yield of silicon is much more matrix dependent than other ion yields (Simon et al., 1991). In this work the ion yield for silicon was adjusted such that the SiO₂ content of a spot measured by ion microprobe and by EDS were in agreement. All other ion yields were held constant. In the Appendix, we use the OB series of mixed rhyolite-basalt glasses to test the assumption that the other ion yields are matrix independent. We find that most ion yields vary by less than 20% through the OB series glasses. As this is much less than the typical concentration difference of a factor of 10 to 20 between the rhyolitic and basaltic endmembers, unaccounted-for variations in ion yield have little effect on the measured diffusion profiles.

Samples RB-2 and RB-3 were later cut perpendicular to their long

axis into a series of slabs about 0.5 mm thick and the ⁴⁴Ca/⁴⁰Ca of each slab measured by thermal ionization mass spectrometry at the Berkeley Center for Isotope Geochemistry using methods described in Russell et al. (1978), Marshall and DePaolo (1982, 1989), and Skulan et al. (1997). Each slab from the diffusion couple was first treated to remove adhering epoxy and then weighed and dissolved as usual in a mixture of HF and HClO₄. The sample weights may have been affected by residual epoxy and hence the Ca concentrations measured for the run products may be slightly low. However, it was also observed that the Ca concentration of the starting basalt measured by isotope dilution (Table 3; 10.38 % as CaO) is about 4% lower than the value measured by wet chemistry and 5% lower than that measured by SEM-EDS. We have not investigated the cause of this discrepancy, since the neither the Ca concentrations measured on the run products nor the precision of the microprobe calibrations at this level is particularly important for our purposes. We consider it unlikely that the SEM-EDS data are incorrect by 5%. The calibration for the EDS is based on a set of well characterized standards and analyses using the same standards give the appropriate CaO concentrations in calcium-bearing minerals known to be stoichiometric. Further investigation of the discrepancy between isotope dilution and microprobe results may be warranted, as isotope dilution has the potential for higher precision and is limited in accuracy mainly by weighing uncertainties. Few comparisons of the two techniques for major elements have been reported.

The calcium isotopic ratios are reported as δ⁴⁴Ca values, which are defined as:

$$\delta^{44}\text{Ca} = \left[\frac{(^{44}\text{Ca}/^{40}\text{Ca})_{\text{sample}}}{(^{44}\text{Ca}/^{40}\text{Ca})_{\text{standard}}} - 1 \right] \times 1000.$$

The standard used is a purified CaCO₃ salt (Skulan et al., 1997). On this scale, the average value of δ⁴⁴Ca measured in 23 samples of volcanic rock (including unpublished data) is -0.12 ± 0.18 ‰. Hence the value

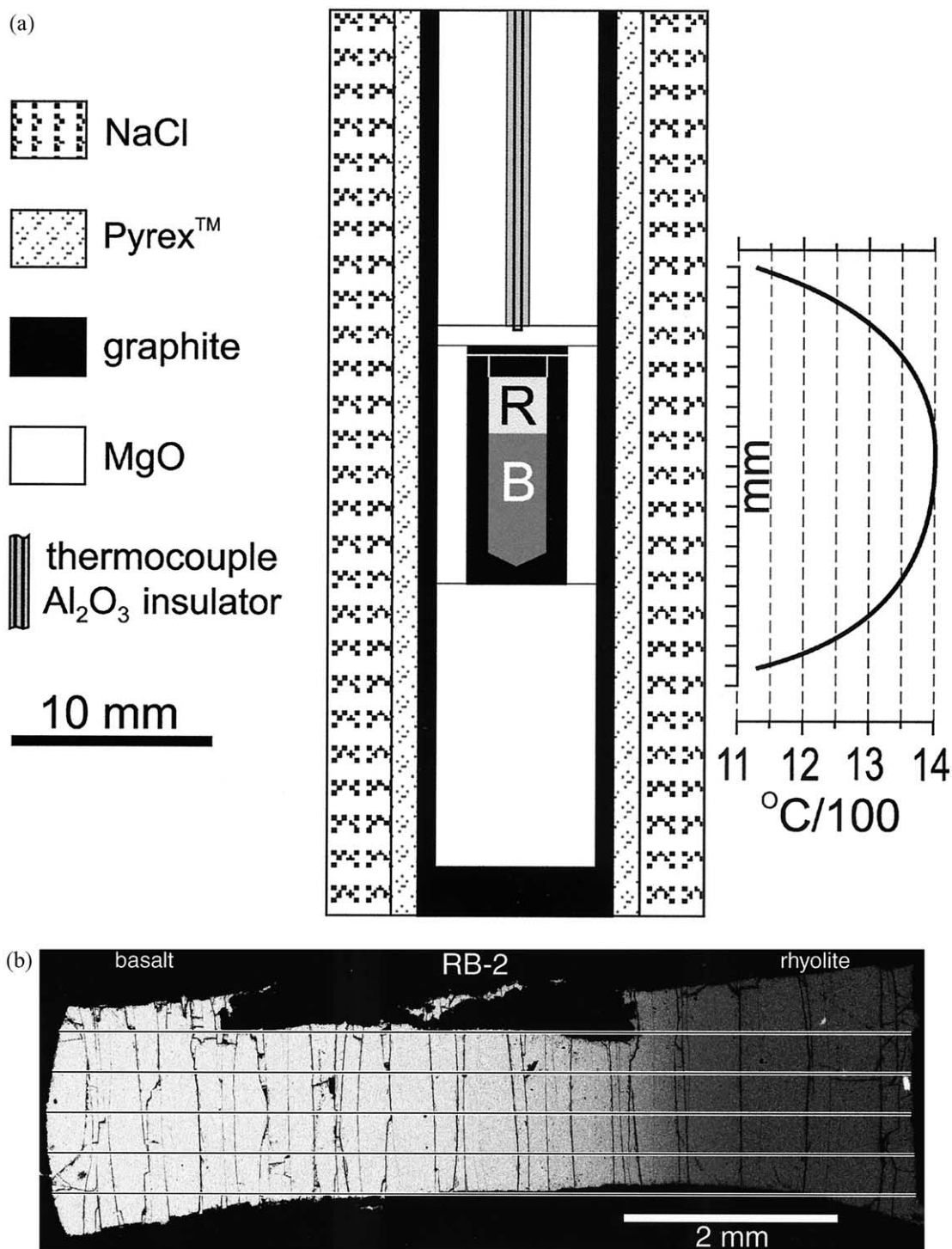


Fig. 1. (a) Schematic diagram of 19-mm diameter piston-cylinder assembly showing the position and dimensions of the rhyolite/basalt diffusion couple. The axial temperature profile depicted at the right was determined at 1400°C and 1.0 GPa for the same assembly lacking only the graphite capsule (see Watson et al., 2002). (b) Backscattered electron image of an exposed portion of glass from sample RB-2. Chemical zoning in the charge is readily apparent, as backscattered electron albedo is proportional to mean atomic number. The silicate charge is surrounded by graphite and the cracks were filled with epoxy when the charge was mounted and polished. Superimposed on the map are five parallel lines indicating where the profiles shown in Fig. 2 were taken.

Table 2. Annealing conditions of the diffusion experiments.

	Temperature (°C)	Pressure (GPa)	Duration (h)	Run-up rate (°C/min)
RB-2	1450	1.3	15.7	75
RB-3	1450	1.2	12.0	75
RB-4	1350	1.2	1.0	135
RB-5	1350	1.2	0.1	270
OB series	1400	1.1	2.0	75

$\delta^{44}\text{Ca} = 0\text{‰}$ is very close the value for an average terrestrial igneous rock. Each value reported in Table 3 represents an average of 2, 3 or 4 mass spectrometer runs. The uncertainties given are calculated from the reproducibility of the multiple measurements and represent an approximation to 95% confidence levels. The average uncertainty is about $\pm 0.13\text{‰}$. The total range measured on natural igneous rock samples to date is -0.33 to $+0.37\text{‰}$.

3. RESULTS

In this section we discuss diffusion profiles from the four experiments listed in Table 2. Figure 2 shows five sets of major element (concentration > 1 wt.%) profiles from sample RB-2, which was annealed for 15.7 h at 1450°C and 1.3 GPa. The five parallel profiles measured for each component are indistinguishable, which is evidence that the diffusive transport was to a very high degree one-dimensional and that the sample suffered no measurable distortion during annealing and quenching. The main source of the obvious asymmetry of these profiles is that diffusion is significantly faster in the basaltic melt than in the rhyolitic one. In the case of the Al_2O_3 profile, and to a lesser degree the Na_2O profile, uphill diffusion is also evident (for a detailed discussion uphill diffusion in silicate melts see Liang

et al., 1997). A remarkable feature of the major element chemical diffusion between basalt and rhyolite is that the effective diffusivities of all the major components are so much alike. This is shown in Figure 3 where the normalized concentration profiles of components not significantly affected by uphill diffusion are compared. The similarity of the effective diffusivity of these components is obvious and especially striking in light of the large differences in the mobility of the major elements in silicate liquids and glasses (see Hofmann, 1980). A similar result was found in $\text{CaO-Al}_2\text{O}_3\text{-SiO}_2$ (CAS) melts where the self diffusion coefficient of calcium is about a factor of ten greater than that of silicon (see Table 5 in Liang et al., 1996a), and yet, the effective diffusivity for SiO_2 and CaO during transport between CAS melts is often indistinguishable (see Figs. 2–4 in Liang et al., 1996b).

The natural abundance of lithium in the basalt and the rhyolite starting materials is quite low, so a small amount of spodumene ($\text{LiAlSi}_2\text{O}_6$), was added to the basalt component of couples RB-3, RB-4, and RB-5 to produce a significant initial concentration gradient in lithium. This resulted in an initial Li concentration of ~ 800 ppm in basalt. The lithium profile in sample RB-3 (12 h at 1450°C) was found to be uniform to within analytical precision, and in RB-4 (1 h at 1350°C), reduced to about half the initial contrast by the exceptionally fast diffusion of lithium. These results led us to anneal sample RB-5 for only six minutes at 1350°C (Fig. 4). The major element profiles in RB-5 are virtually step functions, but the lithium profile extends to the ends of the capsule. Even in this very short run, at the rhyolitic end of the capsule the Li concentration is significantly enhanced relative to the starting composition. Figure 4 provides graphic evidence of the extraordinarily fast diffusion of lithium in natural melts. Note also that there has been some uphill diffusion of lithium and that the uphill diffusion of sodium is more apparent here than it was in RB-2 (Fig. 2).

Table 3. Calcium isotopic measurements from starting materials and diffusion couples RB-2 and RB-3.

Sample	Distance (μm)	Ca (wt.%)	CaO (wt.%)	$\delta^{44}\text{Ca}(\text{‰})$
F-Bas		7.42	10.38	-0.27 ± 0.12
RB3 B6	5000	5.95	8.33	0.96 ± 0.20
RB3 B5	5700	6.22	8.71	0.70 ± 0.22
RB3 B4	6200	6.26	8.76	0.71 ± 0.20
RB3 B3	7700	6.87	9.62	0.82 ± 0.02
RB3 B2	7000	6.60	9.23	0.23 ± 0.03
RB3 R6	3900	5.34	7.48	-0.77 ± 0.05
RB3 R5	3300	4.35	6.08	-0.98 ± 0.23
RB3 R4	2700	1.16	1.62	-2.65 ± 0.11
RB3 R3	1900	0.52	0.72	-5.77 ± 0.18
RB3 R2	1100	0.39	0.55	-2.72 ± 0.23
RB3 R1	250	0.37	0.51	-0.16 ± 0.17
F-Rhy		0.38	0.53	-0.23 ± 0.05
Basalt		7.42	10.38	-0.22 ± 0.03
RB2-1	350	6.27	8.78	1.67 ± 0.17
RB2-2	1000	6.62	9.26	1.08 ± 0.04
RB2-3	1800	6.62	9.26	0.33 ± 0.11
RB2-4	2200	5.71	7.99	-0.10 ± 0.09
RB2-6	3700	6.01	8.41	-0.61 ± 0.28
RB2-8	5000	4.63	6.48	-1.37 ± 0.13
RB2-9	5700	2.41	3.37	-1.47 ± 0.13
RB2-10	6200	0.97	1.36	-4.00 ± 0.17
RB2-11	7000	0.61	0.85	-4.46 ± 0.05
RB2-12	7600	0.51	0.71	-2.44 ± 0.10
Rhyolite		0.38	0.53	-0.24 ± 0.06

Figure 2 shows the high degree of within-run consistency of the measured diffusion profiles. Figure 5 documents the between-run consistency by plotting the concentration data versus normalized distance $X' = X/\sqrt{t}$ where X is the actual distance in microns and t is the annealing time in hours. Figure 5a shows the excellent correspondence between the SiO_2 and CaO profiles from samples RB-2 and RB-3, which were annealed at 1450°C for 15.7 and 12.0 h respectively. Figure 5b compares chemical profiles from samples RB-4 and RB-5 annealed at 1350°C for one hour and for six minutes, respectively. The correspondence between the profiles from RB-4 and RB-5 is particularly important in that it dispels any concern that annealing sample RB-5 for only six minutes might have been too short to develop diffusion profiles that are consistent with those from experiments run for longer times. We do not compare normalized profiles from RB-2 and RB-3 to RB-4 and RB-5 because they were run at different temperatures.

The major purpose of our experiments was to demonstrate and quantify isotopic fractionations during chemical diffusion between natural melts. Calcium isotopic measurements were carried out on the basalt and rhyolite starting materials, and on slabs of glass taken from runs RB-2 and RB-3 (Table 3). Figure 6 shows the $\delta^{44}\text{Ca}$ of the slabs from RB-2 and RB-3 plotted against their average position in normalized distance coordinates: $X' = X/\sqrt{t}$. The $\delta^{44}\text{Ca}$ values of the starting materials

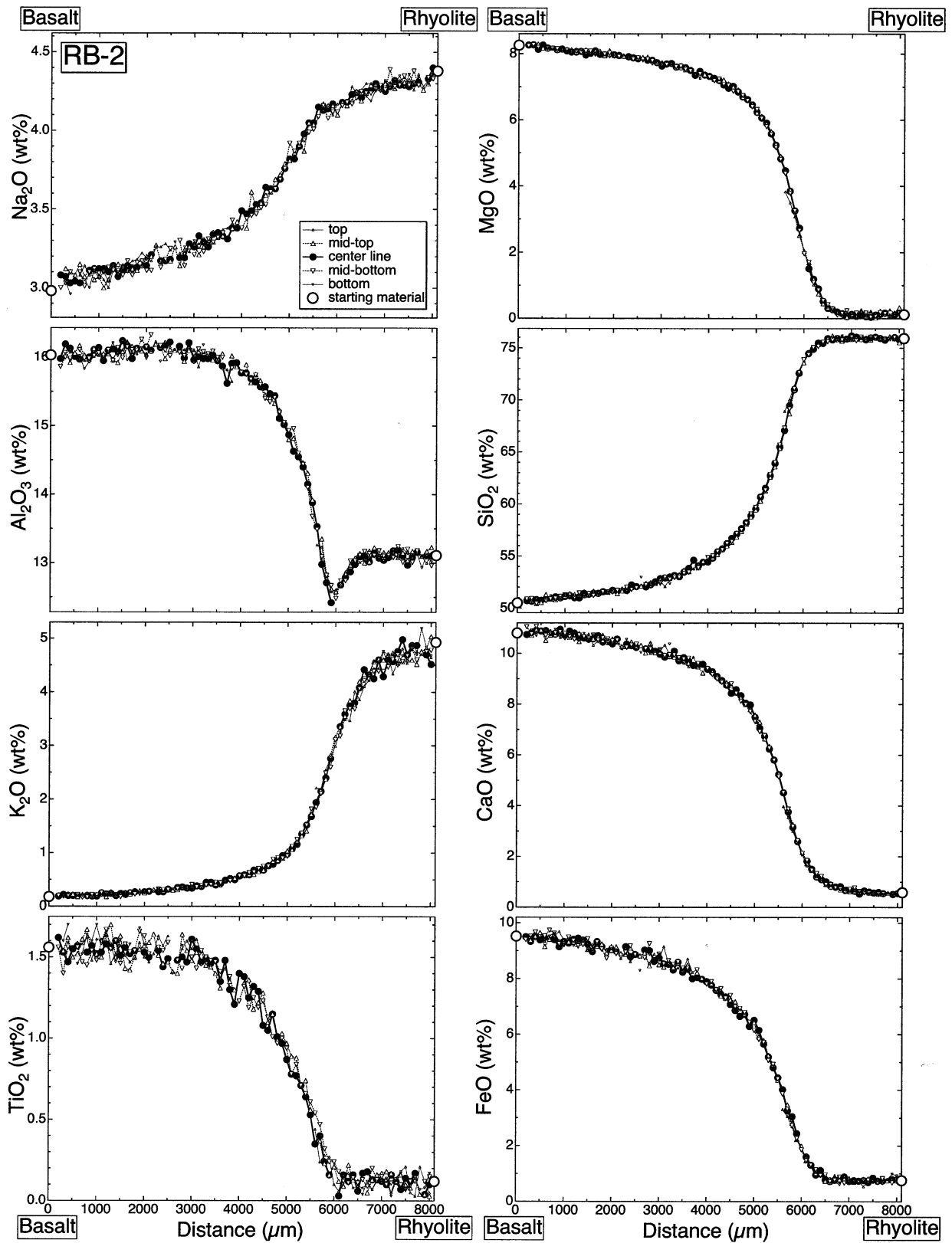


Fig. 2. Major element concentration profiles in wt.% from sample RB-2 (15.7 h at $T = 1450^{\circ}\text{C}$, $P = 1.3 \text{ GPa}$) measured by EDS. Each panel is made up of five separate but parallel profiles, one taken along the centerline and two on each side as shown in Fig. 1b. Although they are difficult to see, there are gaps in the profiles when the lines in Fig. 1b intersect graphite or epoxy.

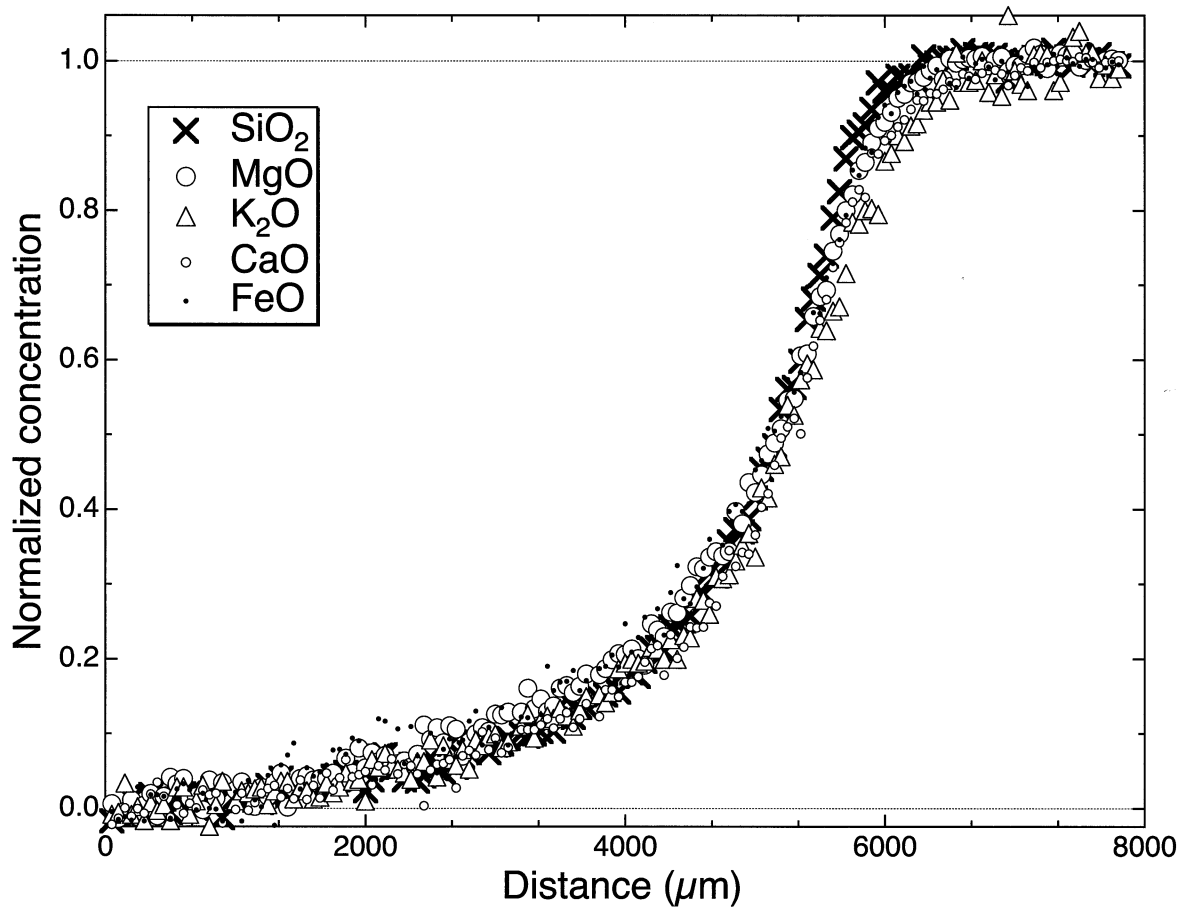


Fig. 3. Normalized concentration profiles of CaO, MgO, K₂O, FeO, and SiO₂ from RB-2 superimposed to show the similarity of the diffusive behavior of these five major components during chemical diffusion between rhyolite and basalt. Concentrations have been normalized by $(C - C_L)/(C_R - C_L)$ where C is the concentration at a point along the profile, C_L is the concentration at the left end of the profile (as seen in Fig. 2), and C_R is the concentration at the right end.

were identical within 0.05 ‰, which is well within the analytical uncertainty, so the diffusion couple was initially isotopically homogeneous throughout. The data show that diffusive transport produced 6 to 7 ‰ variation in $\delta^{44}\text{Ca}$. Both runs show features that are as expected from theoretical considerations (discussed further below). The $\delta^{44}\text{Ca}$ values for the basalt side of the couple are increased relative to the starting compositions, and the $\delta^{44}\text{Ca}$ values in the rhyolite are decreased. In RB-3, the lowest measured value in the rhyolite is about 5.5 ‰ lower than the starting material. For RB-2, the average $\delta^{44}\text{Ca}$ value for the entire couple at the end of the run is equal to the starting value to within 0.05 ‰. For RB-3 the agreement is less good; the end products have a higher $\delta^{44}\text{Ca}$ by 0.3 ‰.

The two sets of calcium isotopic measurements show differences that are well outside of the analytical uncertainties. Run RB-3 shows a pattern that is closer to that expected. The $\delta^{44}\text{Ca}$ values for the basalt side of RB-3 are more or less uniformly increased, although the measured increase is about 1.0 ‰ whereas the predicted value is only about 0.5 ‰. The shape of the $\delta^{44}\text{Ca}$ versus distance curve in the rhyolite part of the couple is close to the theoretical prediction in both amplitude and thickness. The profile for RB-2 departs more markedly

from expectations. The most puzzling part of the RB-2 profile is the steep gradient and high $\delta^{44}\text{Ca}$ values measured near the end of the capsule on the basalt side. The entire profile on the basalt side is significantly different from the model curve. At present we do not have a good explanation for this behavior, but the results are systematic and the size of the variations within the basalt (3 ‰) are far too large to attribute to analytical uncertainties. The extreme high $\delta^{44}\text{Ca}$ values and the steep gradient at the basalt end of the capsule would seem to require either mass loss from this end of the capsule, accompanied by preferential loss of light calcium isotopes, or that the behavior of the calcium transport in the diffusion couple is not entirely captured by the simplified model of independent chemical diffusion of the two isotopes. It may be significant that in RB-2 the effects of diffusion reached both ends of the capsule; the basalt Ca concentration is reduced by about 8% relative to the original, and the basalt side of the couple has substantial gradients in the concentrations of Na, Mg, and K. On the rhyolite end of the couple, the $\delta^{44}\text{Ca}$ value is displaced by -2.2‰ from the starting value, whereas in RB-3 the $\delta^{44}\text{Ca}$ value of the endmost rhyolite sample was not measurably changed.

Figure 7 shows $^7\text{Li}/^6\text{Li}$ measured with the University of

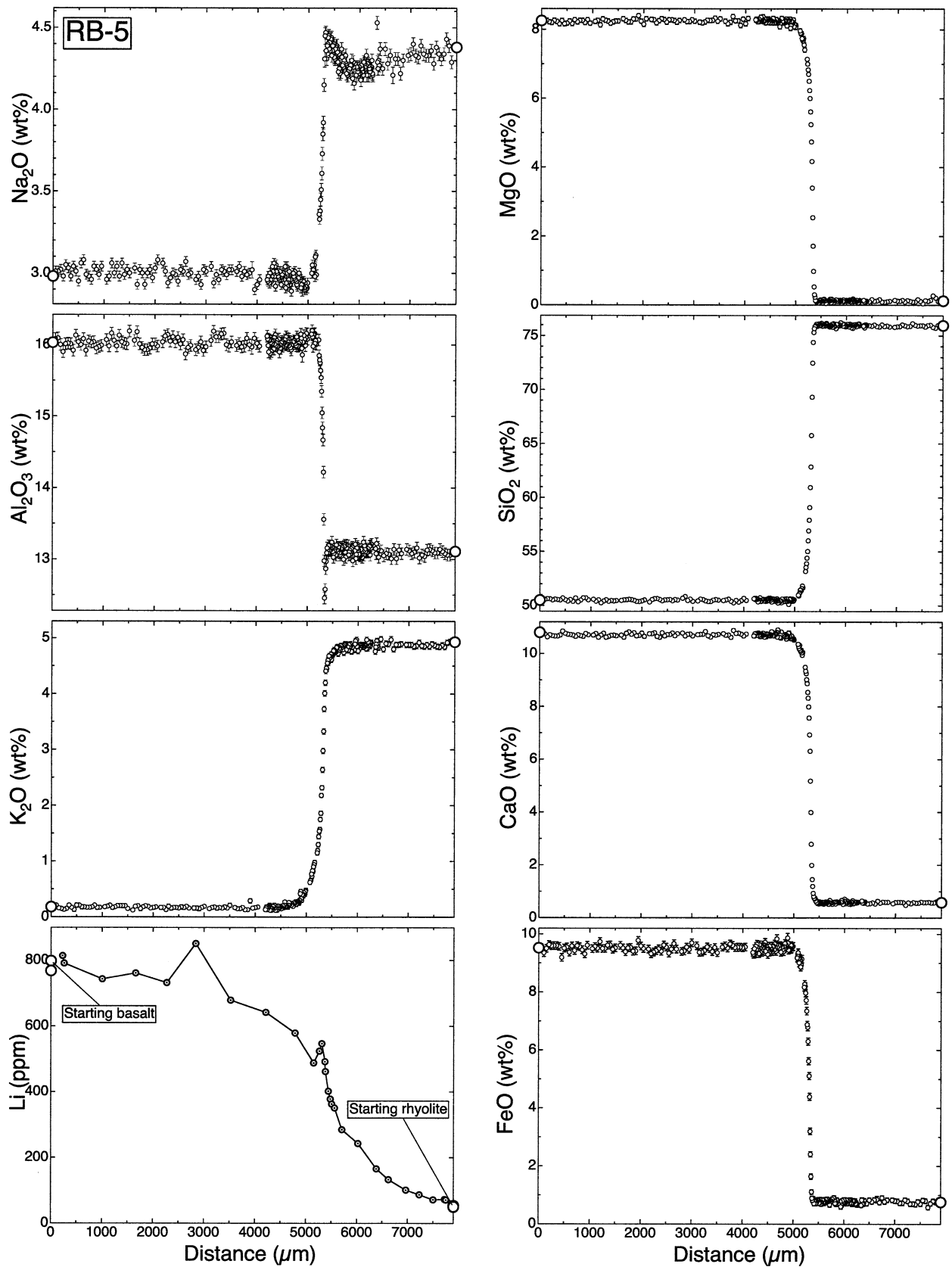


Fig. 4. Same as Fig. 2 except that the annealing conditions are now only 6 min at $T = 1350^{\circ}\text{C}$, $P = 1.2\text{GPa}$ and what was the TiO₂ panel has been replaced by a profile of Li concentration measured by ion microprobe. Two measurements of the Li concentration in the starting basalt and four virtually identical measurements of Li in the starting rhyolite are plotted. The values reported in Table 1 are the averages of these measurements. The uphill diffusion of Na₂O is now more obvious than it was in RB-2, but the most dramatic feature of these profiles is the contrast between lithium and all other profiles, showing how much more rapidly lithium diffuses.

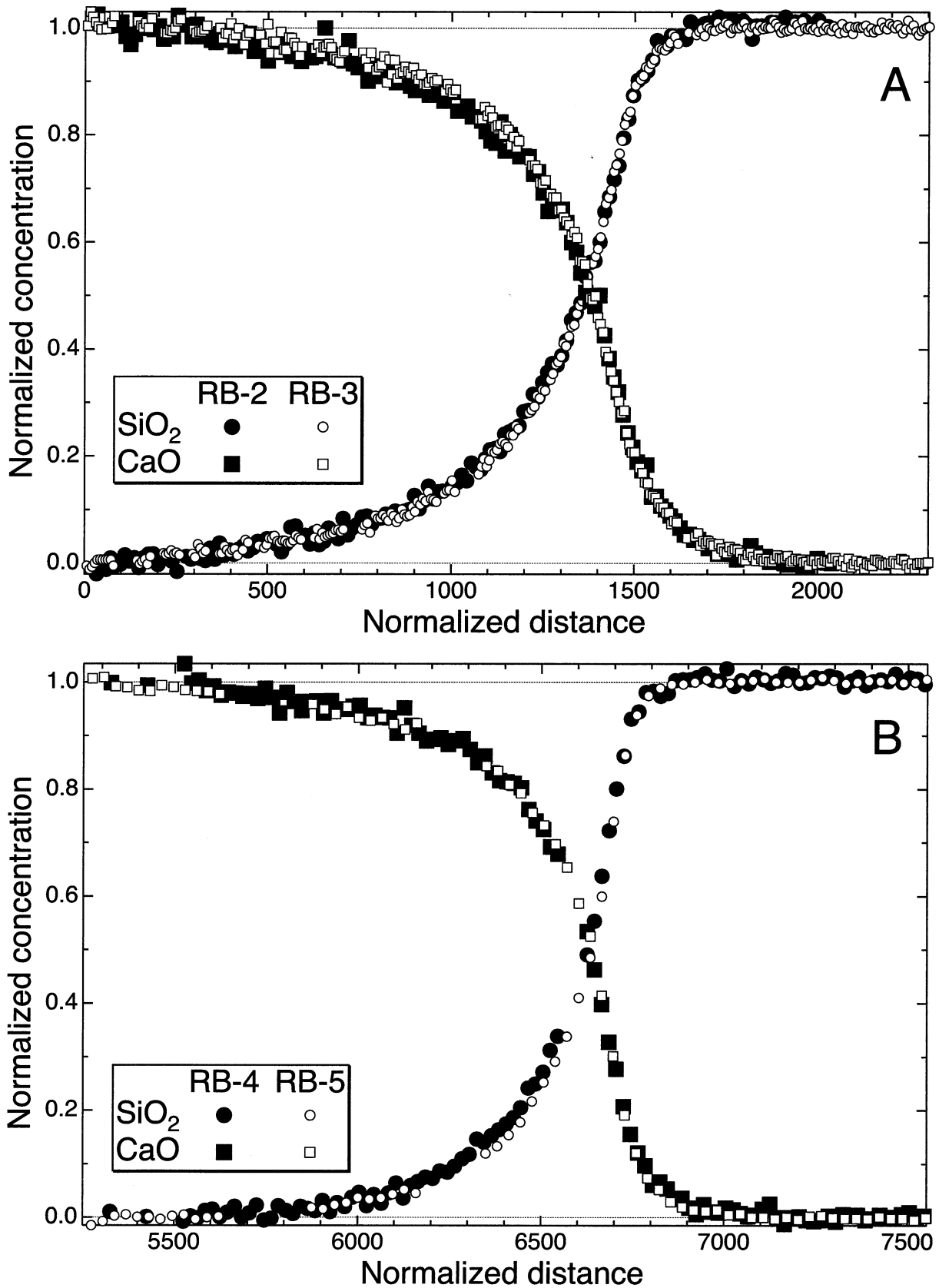


Fig. 5. Normalized concentration profiles (as in Fig. 3) from RB-2, RB-3, RB-4, and RB-5 plotted against normalized distance $X' = X/\sqrt{t}$, where X is the distance along the profile in μm and t is run duration in hours. Panel (a) compares the SiO₂ and CaO profiles from RB-2 and RB-3. Panel (b) compares the SiO₂ and CaO profiles from RB-4 and RB-5.

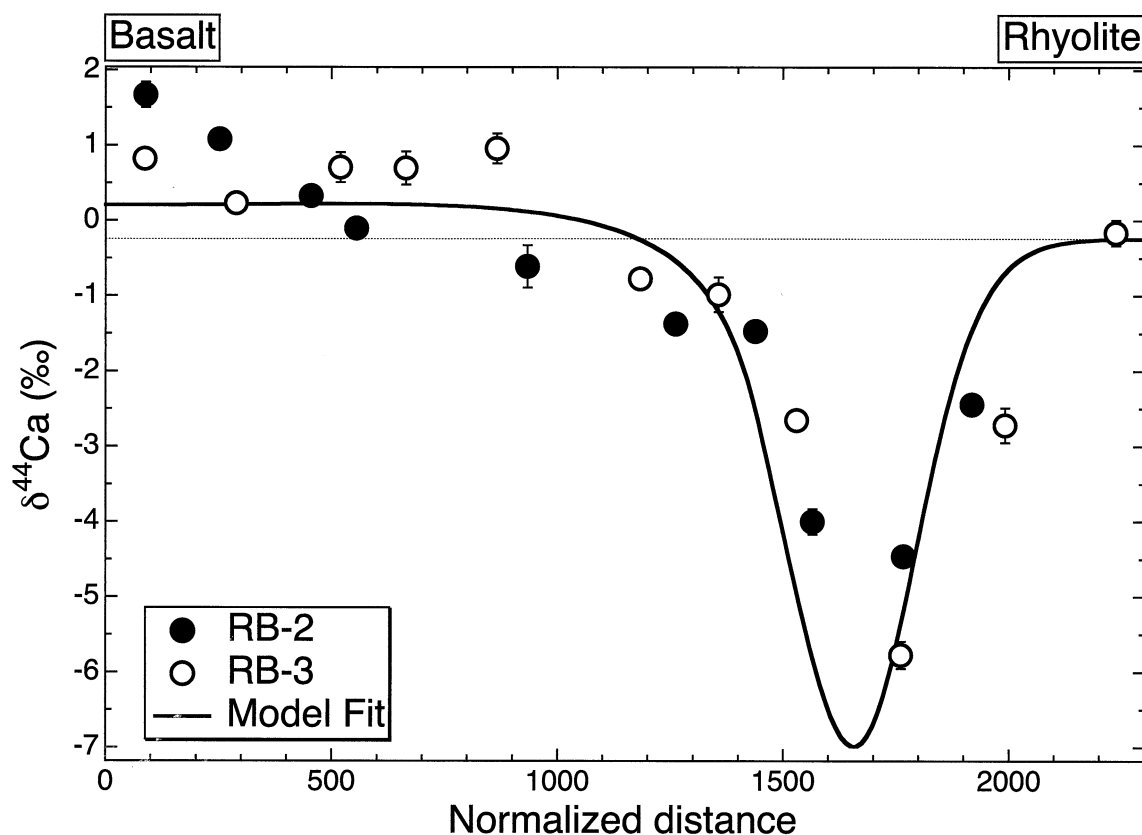


Fig. 6. $^{44}\text{Ca}/^{40}\text{Ca}$ measured on materials taken from samples RB-2 and RB-3 plotted as $\delta^{44}\text{Ca}$ versus normalized distance $X' = X/\sqrt{t}$, where X is the distance along the profile in μm and t is run duration in hours. The dashed line joins the starting isotopic compositions of basalt and rhyolite given in Table 3. Also shown is a model curve calculated using $\beta=0.075$ (see Eqn. 5).

Chicago ion microprobe, at various points along the lithium diffusion profile from sample RB-5 (see Fig. 4). The diffusion of lithium from the basalt to the rhyolite fractionated ^7Li from ^6Li by several tens of ‰, which is easily resolved given an analytic precision of $\pm 5\%$. There appears to be a difference between starting rhyolite and basalt of $\sim 20\%$, which we take into account when modeling the Li diffusion data. There can be matrix effects on the ion microprobe isotopic measurements. However, the chemical composition of RB-5 is essentially basaltic or rhyolitic from the ends of the charge to fairly close to the interface (Fig. 5). Thus, if there were a significant matrix effect on $\delta^7\text{Li}$, there should be a sudden shift at the interface. The data do not show such a sudden shift. Note that unlike calcium, where there is a large negative peak $\sim 500\ \mu\text{m}$ from the interface and the ends of the sample charge have close to the initial calcium isotopic composition (Fig. 6), $\delta^7\text{Li}$ decreases continually from the interface to the end of the charge. As we shall see in the next section, this is likely due to a significant amount of diffusively fractionated lithium having reached the rhyolitic end of the capsule.

The diffusion profiles from RB-5 (Fig. 4) clearly show that lithium diffuses exceptionally fast compared to the major elements. To check whether this exceptional behavior of lithium might be due to its very low concentration (i.e., tracer diffusivity vs. chemical diffusivity) we also measured diffusion profiles of a large number of other trace components (see

Appendix). The effective diffusion coefficients of all these trace elements were very similar to that of the major elements and thus also several orders of magnitude smaller than that of lithium.

4. MODEL CALCULATIONS

In this section we use model calculations to quantify the kinetic isotopic fractionation factors for calcium and lithium. The fractionation factors are determined by comparing the results of model calculations to the measured elemental and isotopic profiles.

The mathematical representation of the one-dimensional chemical diffusion problem (Onsager, 1945) involves conservation equations of the form

$$\frac{\partial C_i}{\partial t} = -\frac{\partial J_i}{\partial X'} \quad (1)$$

where C_i is the molar density (moles cm^{-3}) of component i , and J_i is the molar flux (moles $\text{cm}^{-2}\ \text{s}^{-1}$), together with constitutive equations of the form

$$J_i = -\sum_{j=1}^{n-1} D_{ij} \frac{\partial C_j}{\partial X'} \quad (2)$$

where for an n -component system, the sum in j is taken over

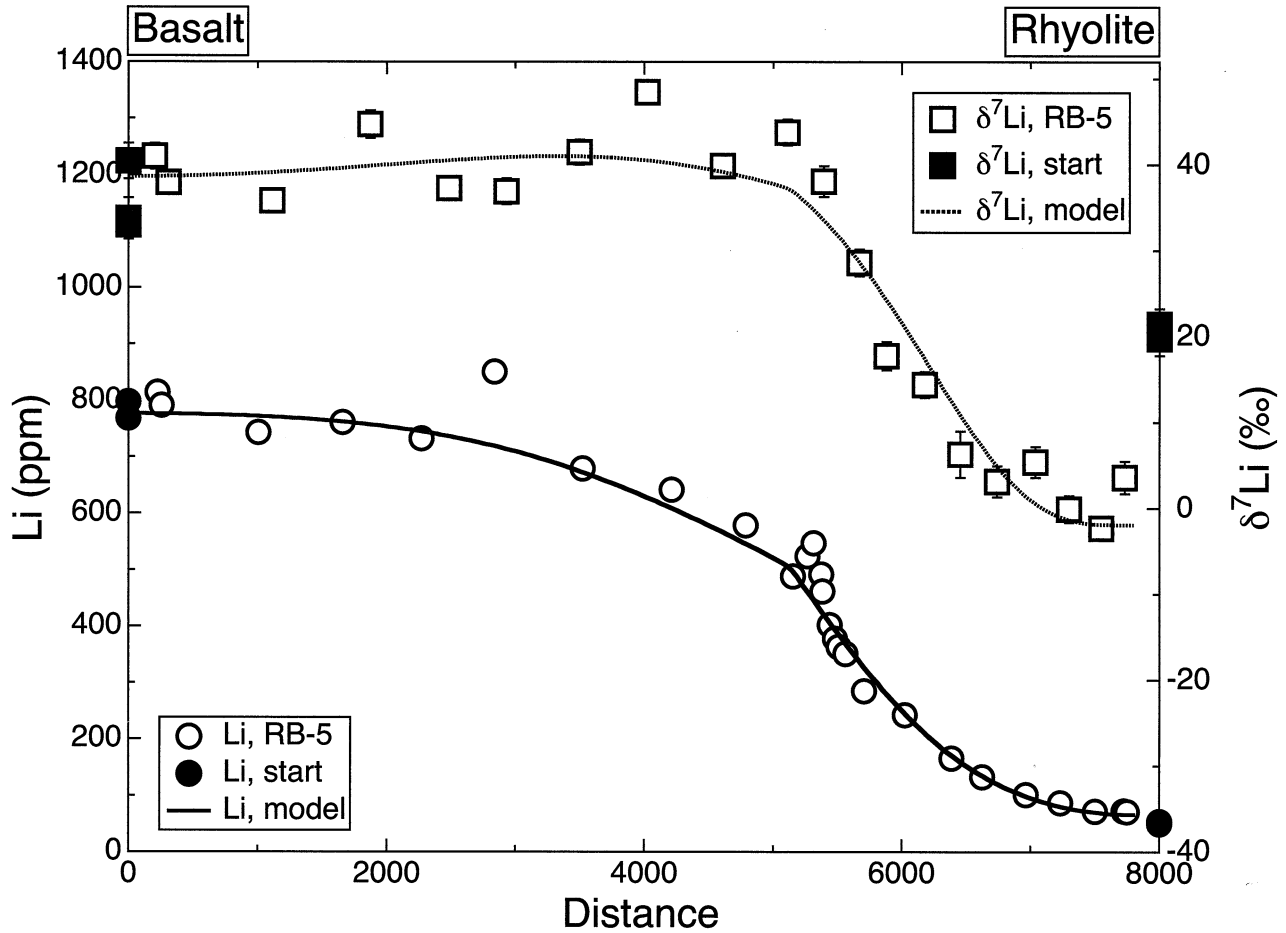


Fig. 7. $\delta^7\text{Li}$ and Li concentrations measured by ion probe on materials from sample RB-5 plotted vs. normalized distance. Also shown are the initial concentration and isotopic composition of the basalt and rhyolite and model curves. The model curve used to fit to the Li concentration data assumed a diffusivity $D_{\text{Li}} = 6 \times 10^{-5} e^{-4(X_{\text{SiO}_2}-0.5)} \text{ cm}^2 \text{ s}^{-1}$, where X_{SiO_2} is the weight fraction of SiO_2 in the melt. The model curve used to fit the $\delta^7\text{Li}$ data was calculated using $\beta = 0.215$.

$n-1$ independent components and D_{ij} are the elements of a multicomponent diffusion matrix. The appropriate boundary conditions for our purpose are

$$\frac{\partial C_i}{\partial x} = 0 \text{ at } x = 0, L, \quad (3)$$

corresponding to no flux at the ends $x = 0$ and $x = L$ of the sample capsule. The diffusion matrix for a molten rhyolite-basalt system has yet to be determined, thus we are forced to resort to the common simplification of using a single effective diffusion coefficient for each component. Eqn. 2 is replaced by

$$J_i = -D_i \frac{\partial C_i}{\partial x} \quad (4)$$

and we will allow the coefficients D_i to be functions of the SiO_2 content of the melt as needed to fit the asymmetry of those diffusion profiles that do not show obvious uphill diffusion. The use of Eqn. 4 in place of Eqn. 2 is better justified than usual in the present application because we are restricting our interest to diffusion in a particular direction in composition space (see Cooper, 1965, for the relationship between the effective diffu-

sion coefficients, the elements of the diffusion matrix, and direction in composition space). Eqn. 4, with D_i depending on the local SiO_2 content, is justified a posteriori by our model calculations showing that it provides a representation of the chemical fluxes that can account for the evolution of the major element concentrations in both space and time.

We are particularly interested in determining a parameter that will, in a generalizable way, characterize the diffusive fractionation of calcium and lithium isotopes in natural silicate melts. In the absence of any theoretical basis for choosing a particular functional form for the relationship between the diffusivity and the mass of components of a silicate liquid, we will assume, following Richter et al. (1999), that ratio of the effective diffusion coefficients of the isotopes 1 and 2 of element i are related to their masses by

$$\frac{D_{i,1}}{D_{i,2}} = \left(\frac{m_{i,2}}{m_{i,1}} \right)^\beta, \quad (5)$$

where β is an empirical parameter to be determined from the experimental data.

The necessary first step for modeling the diffusion profiles

from the basalt-rhyolite couples involves fitting the SiO₂ data, which, given our formulation of the problem, involves finding the dependence of the effective diffusivity of SiO₂ on the SiO₂ content of the melt. Once a good fit has been achieved to the SiO₂ data, we can proceed to modeling the profiles of the other major components using diffusion coefficients that depend on the known evolution of the SiO₂ concentration. We employed a commonly used approach for finding the compositional dependence of the diffusion coefficients, the Boltzmann-Matano method (see Sherwon, 1963), where the diffusion coefficient D as a function of composition c' is given by

$$D(c') = -\frac{1}{2t} \left(\frac{dx}{dc'} \right) \int_{c_1}^{c'} x dc. \quad (6)$$

x is distance measured relative to the plane $x=0$ defined by

$$\int_{c_1}^{c_2} x dc = 0, \quad (7)$$

c_1 and c_2 are the values of c' at the ends of the diffusion couple, and $(dx/dc')_{c'}$ is evaluated at $c=c'$ with data from the diffusion profile at time t . Using Eqn. 6 to determine the dependence of the diffusion coefficients on the silica content of the melt is not straightforward because the derivative involved is extremely sensitive to inaccuracies in the data, especially if the data are closely spaced as is the case here. Unrealistic fluctuations in $D(c')$ can be reduced by smoothing the diffusion profiles before evaluating $(dx/dc')_{c'}$, which we do by truncating the Fourier series representations of the profiles at twenty terms and then calculating the derivatives from the Fourier coefficients. Even so, significant fluctuations in $D(c')$ remain once c' approaches the far field values c_1 and c_2 , and dx/dc' becomes large. Because the results of using the Boltzmann-Matano method depend on how one chooses to smooth the concentration data, we use it only as first estimate of the dependence of the diffusivities on SiO₂ content. We then use trial and error to further refine the diffusion coefficients until we achieve a desired level of fit between calculated and measured data.

Figure 8 shows the fit of calculated diffusion profiles for SiO₂, CaO, and K₂O to data from diffusion couple RB-2. The parametric form used for the dependence of the diffusion coefficients on the weight fraction of SiO₂ in the melt is

$$D_{\text{SiO}_2} = D_0 e^{-\alpha(X_{\text{SiO}_2} - 0.5)} + D_1, \quad (8)$$

where D_0 is the diffusion coefficient when SiO₂ = 50 wt.% (i.e., $X_{\text{SiO}_2} = 0.5$), α specifies the sensitivity of the diffusion coefficient to changes in the SiO₂ content of the melt, and D_1 is a lower bound for the diffusivity when the SiO₂ content exceeds 68%. The values of α , D_0 , and D_1 that were used to effect the fits shown in Figure 8 are $\alpha = 12.0$, $D_0 = 4 \times 10^{-7} \text{ cm}^2 \text{ s}^{-1}$, and $D_1 = 0 \text{ cm}^2 \text{ s}^{-1}$ for SiO₂; $\alpha = 14.5$, $D_0 = 8 \times 10^{-7} \text{ cm}^2 \text{ s}^{-1}$, and $D_1 = 4 \times 10^{-8} \text{ cm}^2 \text{ s}^{-1}$ for CaO; $\alpha = 10.0$, $D_0 = 6 \times 10^{-7} \text{ cm}^2 \text{ s}^{-1}$, and $D_1 = 0 \text{ cm}^2 \text{ s}^{-1}$ for K₂O. These parameters will give an equally good fit to data from RB-3, since we have already shown that these are equivalent to those of RB-2 once the difference in run duration is taken into account.

Figure 6 shows data from diffusion couples RB-2 and RB-3

indicating significant isotopic fractionation associated with the diffusion of calcium from molten basalt to molten rhyolite. Also shown Figure 6 is a model ⁴⁴Ca/⁴⁰Ca profile calculated using $\beta = 0.075$ in Eqn. 5. The pronounced local minimum in ⁴⁴Ca/⁴⁰Ca is the result of the faster diffusion of ⁴⁰Ca relative to ⁴⁴Ca into the rhyolite. Since the magnitude of the isotopic fractionation is, to a good approximation, proportional to β , the data shown in Figure 6 are sufficient to constrain β to be in the range 0.05–0.1. This is the same range of β reported by Richter et al. (1999) for the relative mobility of calcium isotopes in a simpler isochemical silicate melt. Our finding that calcium isotopes fractionate during chemical diffusion between molten rhyolite and basalt in much the same way they do in an isochemical CAS melt leads us to believe that Eqn. 5 with $\beta = 0.05$ –0.1 is a generally applicable measure of the relative mobility of calcium isotopes in molten silicate systems.

Lithium isotopes can be very significantly fractionated by diffusion between silicate melts (Fig. 7). What we did not anticipate, but Figure 4 makes very clear, is how much more rapidly lithium diffuses in silicate melts compared to all other major and trace elements that we analyzed. Also shown in Figure 7 are calculated lithium isotopic and concentration profiles compared to data from couple RB-5. The diffusion parameters for lithium used in connection with Eqn. 8 are $\alpha = 4.0$, $D_0 = 6 \times 10^{-5} \text{ cm}^2 \text{ s}^{-1}$, and $D_1 = 0 \text{ cm}^2 \text{ s}^{-1}$. The calculated isotopic profile shown in Figure 7 is from a model using these diffusion parameters and $\beta = 0.215$.

The contrast between the behavior of lithium and calcium during diffusion between molten basalt and rhyolite is quite dramatic in terms of the magnitude of the respective diffusion coefficients, their dependence on the silica content of the melt, and the factor β . The effective diffusion coefficient for lithium is about 100 times larger than that for calcium in a melt with 50 wt.% SiO₂, and almost 1000 times larger for 70 wt.% SiO₂. That lithium isotopes are much more fractionated by diffusion than the isotopes of calcium we measure, is due in part to their larger mass ratio ($7/6 = 1.166$ vs. $44/40 = 1.100$), but more so because of the much larger kinetic fractionation parameter of lithium ($\beta_{\text{Li}} \approx 0.215$ vs. $\beta_{\text{Ca}} \approx 0.075$).

5. SUMMARY AND DISCUSSION

Diffusion couples juxtaposing molten rhyolite and basalt were used to demonstrate that calcium and lithium isotopes can be significantly fractionated by chemical diffusion between natural composition melts. The magnitude of kinetic isotope fractionations is a function of both the degree to which the diffusivity of isotopically distinct components depends on mass (i.e., the parameter β) and on the concentration differences driving diffusion. The dependence of the isotopic fractionation on β and concentration contrast is illustrated in Figure 9, which is a modified version of Figure 8 of Richter et al. (1999). Included in this figure are points indicating the conditions and isotopic fractionation of calcium and lithium reported here. Also shown are predictions for the likely magnitude of isotopic fractionations of the isotopes of other major elements such as potassium, magnesium and iron, and the minor element titanium, given the contrast in their concentrations in the rhyolite and basalt we used as starting materials. In order for these measured or predicted isotopic fractionations to be useful mon-

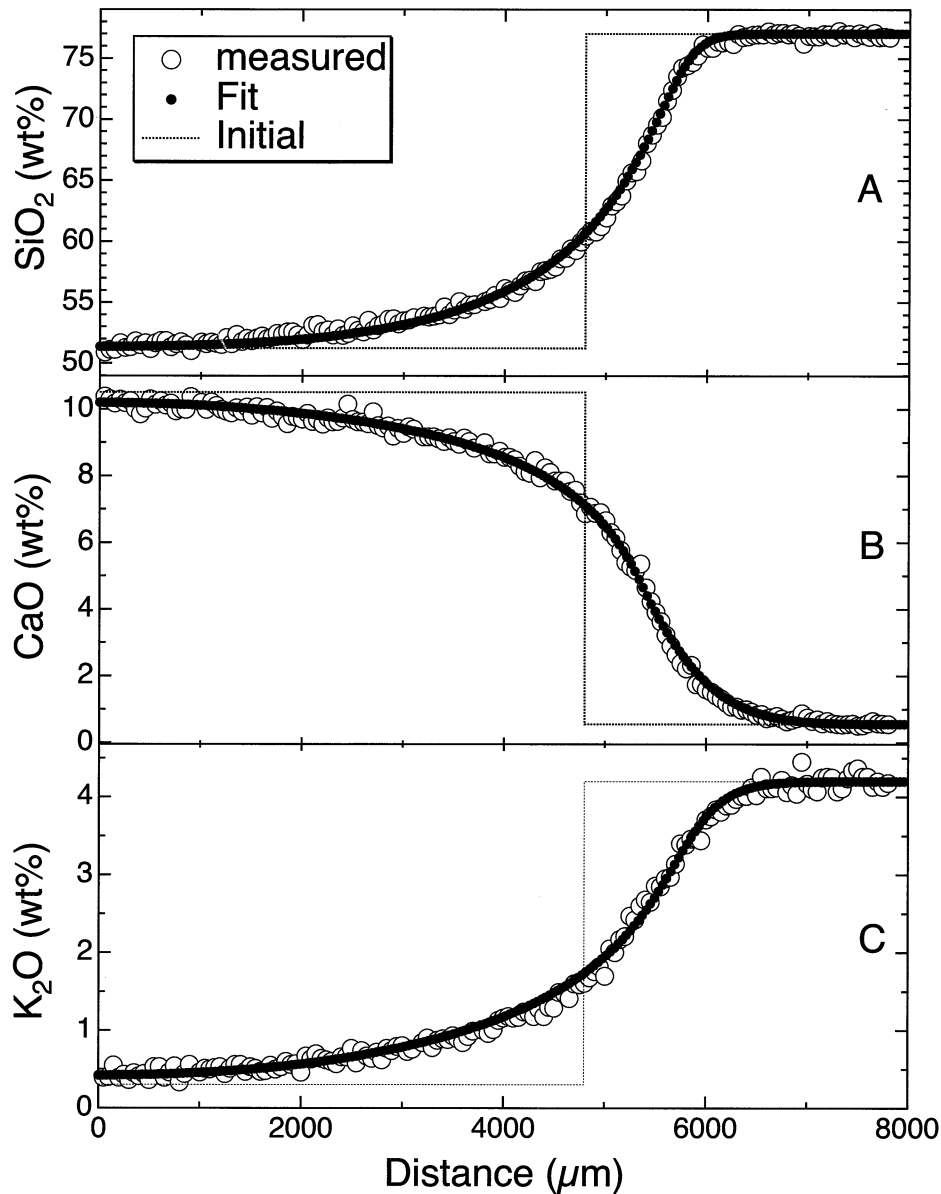


Fig. 8. Model fits to the measured diffusion data from diffusion couple RB-2: (a) SiO_2 , (b) CaO , and (c) K_2O . The dependence of the diffusion coefficients D on the SiO_2 weight fraction X_{SiO_2} is specified to be of the form $D(\text{SiO}_2) = D_0 e^{-\alpha(X_{\text{SiO}_2} - 0.5)} + D_1$ with $D_0 = 4 \times 10^{-7} \text{ cm}^2 \text{ s}^{-1}$, $D_1 = 0$, $\alpha = 12.0$ used to fit the SiO_2 data; with $D_0 = 8 \times 10^{-7} \text{ cm}^2 \text{ s}^{-1}$, $D_1 = 4 \times 10^{-8} \text{ cm}^2 \text{ s}^{-1}$, $\alpha = 14.5$ used to fit the CaO data; and $D_0 = 6 \times 10^{-7} \text{ cm}^2 \text{ s}^{-1}$, $D_1 = 0$, $\alpha = 10.0$ used to fit the K_2O data.

itors of the mode of chemical transport in natural systems they will have to be large not only with respect to analytical precision, but also large compared to isotopic variations that might arise from other causes such as the mixing of isotopically distinct components. This latter requirement seems likely to be met for a number of important chemical systems given that the range of isotopic variations in calcium (see Marshall and De Paolo, 1989; Table 1), iron (see Beard and Johnson, 1999; Table 1), potassium (see Humayun and Clayton, 1995; Table 3), and lithium (see James and Palmer, 2000; Table 3) so far measured in a relatively broad range of silicate rocks are small compared to the magnitude of kinetic fractionations that we

predict for a sufficiently large contrast in the elemental concentration. High precision measurements of magnesium isotope variations among terrestrial rock types are not yet available, but the ability to make such measurements has recently been demonstrated by Galy et al. (2001).

The results we have reported here clearly demonstrate that diffusion between natural melt compositions can measurably fractionate the isotopes of calcium and lithium, and we see no reason why the same sort of fractionations should not occur in appropriate natural settings. The only published reports that we are aware of claiming isotopic fractionation by chemical diffusion in a natural silicate system involve the diffusion of

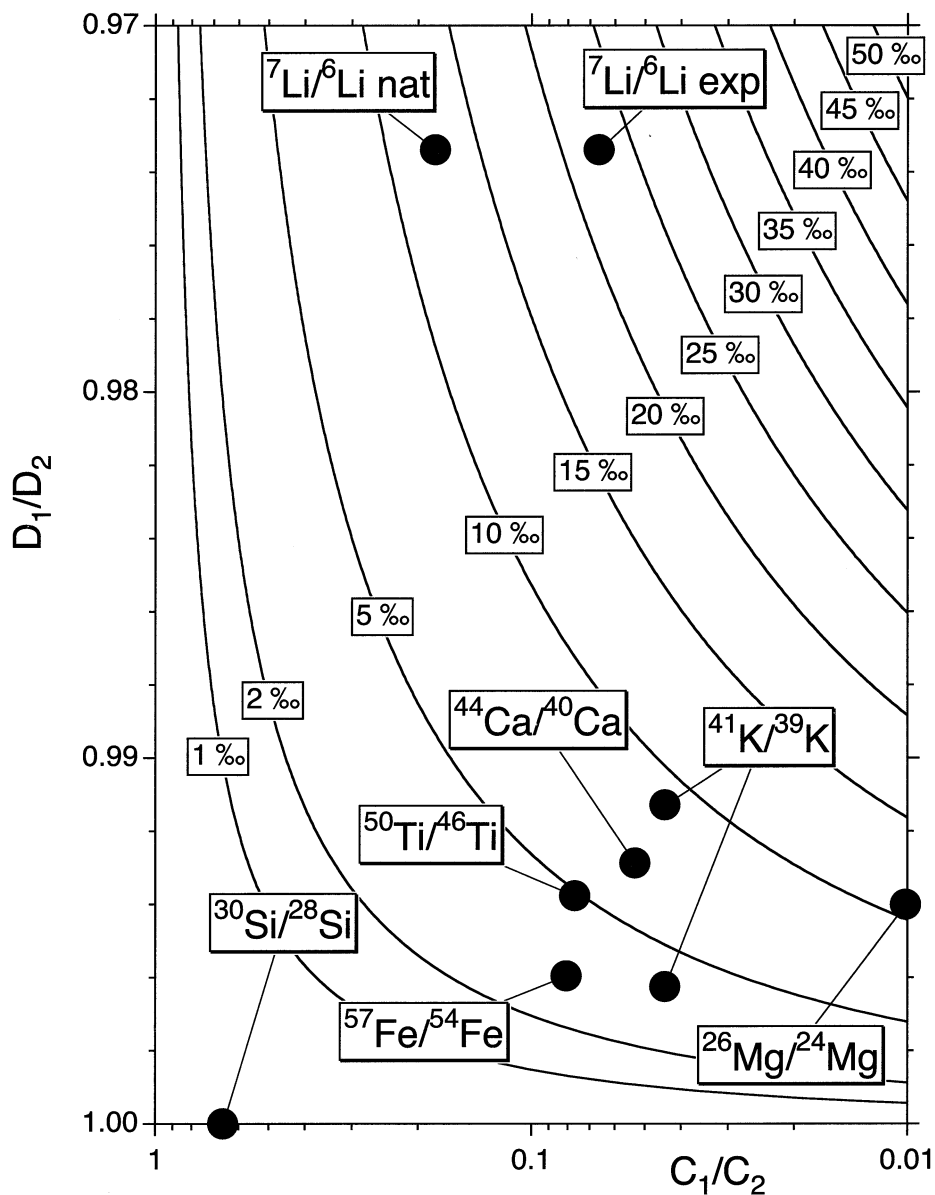


Fig. 9. Contours of calculated isotope fractionation by diffusion between two silicate liquids as a function of the ratio of the elemental concentrations and of the ratio of the diffusivity of the isotopes. Also shown are the results of our experiments for lithium and calcium isotope fractionation and expected fractionation for a number of other isotopic ratios. The experimental result for lithium isotope fractionation involved a lithium-doped basalt and thus an artificially high concentration contrast. A second point (${}^7\text{Li}/{}^6\text{Li}$ nat) is plotted for the expected isotopic fractionation of lithium using the concentration ratio of natural basalt and rhyolite. The diffusion ratios for magnesium, iron, and titanium isotopes were calculated assuming $\beta = 0.075$ as was found for calcium. Two points are plotted for the potassium isotopes. The point with the smaller predicted fractionation has a diffusion ratio based on $\beta = 0.075$ (as for calcium) while the point with the larger fractionation used $\beta = 0.215$ (as for lithium). For silicon we used $\beta = 0$ assuming that germanium is a good analog for silicon and the Richter et al. (1999) value, $\beta < 0.025$ for germanium.

potassium. Schreiner and Verbeek (1965) report variations in the ${}^{39}\text{K}/{}^{41}\text{K}$ ratio of several tens of per mil in the vicinity of a granite-shale contact. However, when Humayun and Clayton (1995) remeasured the potassium isotopic composition of selected samples from the Schreiner and Verbeek (1965) set, they found no isotopic fractionations of the ${}^{41}\text{K}/{}^{39}\text{K}$ ratio greater than about 1‰. The concentration of K in both the granite and in the shale are in the range of 3–4%, thus based on Figure 9 we would not expect there to have been any measurable isoto-

pic fractionation due to diffusion. Verbeek and Schreiner (1967) report large potassium isotopic fractionations (as much as -29% in ${}^{41}\text{K}/{}^{39}\text{K}$) in the contact zone between granite and amphibolite. What is tantalizing about this particular report is that the spatial distribution of the isotopic variations is a narrow local minimum similar to that in Figure 6. However, the magnitude of the reported fractionations is so large as to require an unrealistic value for β (i.e., $\beta > 1/2$) for any reasonable choice of the K concentration contrast between the granite and the

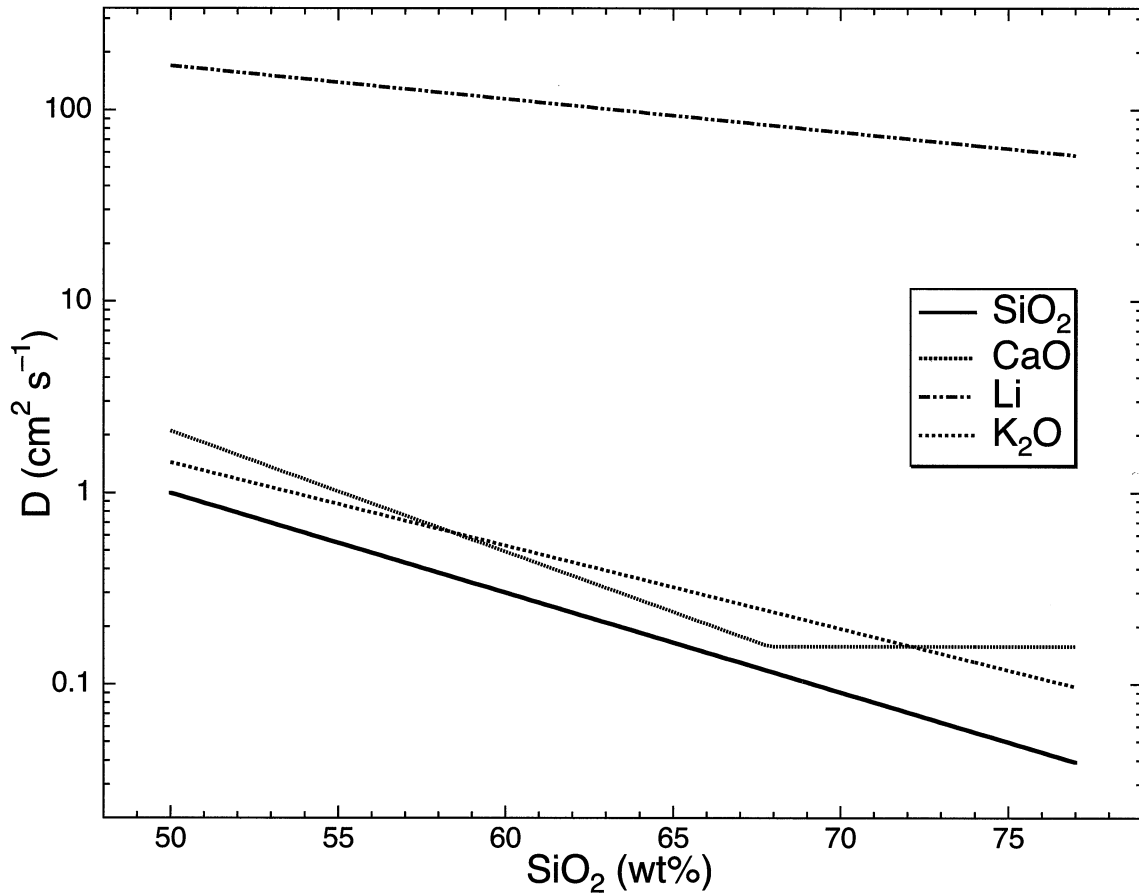


Fig. 10. Effective diffusivity of Li, CaO, K₂O, and SiO₂ as a function of the SiO₂ content of the melt used to affect the fits to the measured data shown in Figs. 8 and 9.

amphibolite. It seems very likely that there are also serious problems with the isotopic measurements reported by Verbeek and Schreiner (1967) and therefore we cannot accept their claim of having found a field example of kinetic isotope fractionation by chemical diffusion. While disappointing, we hope that this conclusion will not deter future studies of kinetic isotope fractionation in natural systems given the greater precision and reliability of modern analytical methods and our demonstration that diffusion under appropriate circumstances can indeed produce measurable isotopic fractionations.

The effective diffusion coefficients that we used to characterize chemical transport between rhyolite and basalt melts are in some cases consistent with previous studies, but in others quite interestingly different. The SiO₂ diffusion parameters that give a good fit to the RB-2 data are similar to those one calculates using the Leshner (1994) parameterization ($\alpha = 12.28$, $D_0 = 2.2 \times 10^{-7} \text{ cm}^2 \text{ s}^{-1}$ at 50 wt.% SiO₂ and $T = 1450^\circ\text{C}$) for the diffusivity of SiO₂ between anhydrous basalt and rhyolite. The D_0 we used for calcium is similar to the effective diffusion coefficient for a mugearite melt reported by Medford (1973). We hasten to add that this agreement should not be taken to imply that our results regarding the diffusion coefficients can be generalized on the basis of silica content alone. For example, differences as large as a factor of ten have been reported for the diffusion coefficient of SiO₂ in melts with

the same SiO₂ content (Watson, 1982). That melts with similar SiO₂ content may differ very significantly in their diffusive properties is most likely due to the chemical potentials being significantly affected by the concentration of components other than SiO₂.

Arguably, the most remarkable finding regarding the effective diffusion coefficients is the distinctiveness of the diffusive behavior of lithium compared to all other elements we have analyzed. Figure 4 gives qualitative but dramatic evidence of exceptional rapidity of lithium diffusion relative to the major components of the melt. Figure 10 compares the diffusion coefficients for SiO₂, CaO, K₂O, and Li as a function of the SiO₂ content of the melt. The diffusion coefficient of lithium is about two orders of magnitude larger than that of the other components in basaltic compositions and almost three orders of magnitude larger in rhyolite. To address the question of whether this large difference in diffusivity might be the result of our comparing a trace component, lithium, to major components of the melt, we used the ion microprobe to also measure diffusion profiles of a number of other trace elements. Profiles of a number of trace elements are shown in Figure 11. Many more trace elements were measured, but could not be used to calculate effective binary diffusion coefficients, because: (1) concentrations in the two endmembers were too similar (Y, Pr, Nd, Sm, Eu); or (2) significant uphill diffusion occurred (Be,

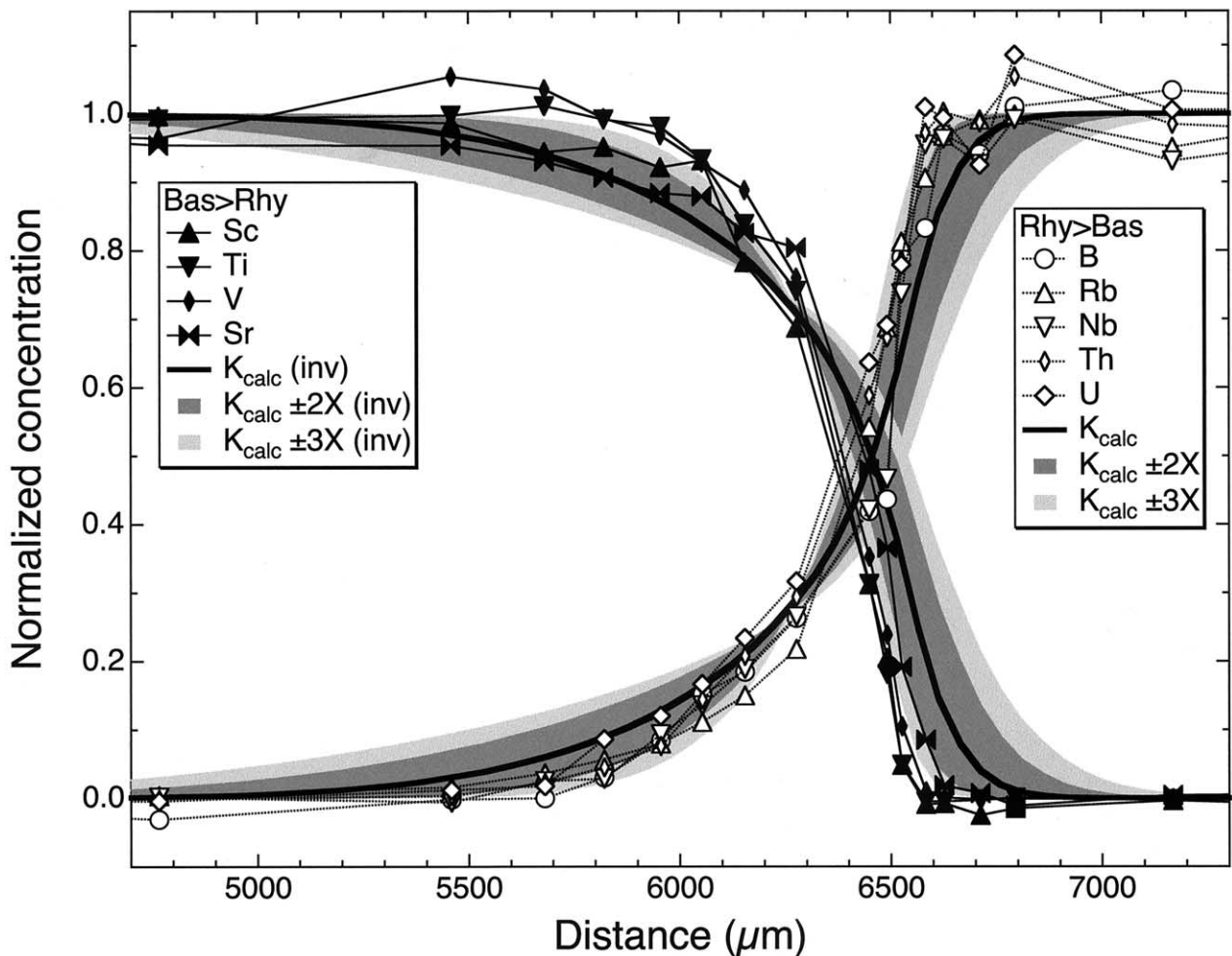


Fig. 11. Profiles of selected trace elements in RB-4. These profiles were used to infer the effective diffusivities of trace elements shown in Fig. 12. The profiles were normalized to endmember compositions for ease of comparison. Also shown are fits to potassium measured in RB-2 by EDS, along with curves calculated for the diffusivity multiplied and divided by factors of two and three. Most trace elements have lower diffusivities than potassium.

Mn, Ba). Details regarding the ion microprobe measurements and the use of standards to determine and correct for matrix effects is given in an Appendix. We find that lithium is exceptional even when compared to a broad range of trace elements. In Figure 12 we show this by plotting the diffusion coefficients of selected major and trace elements vs. z^2r , where z is charge and r is the ionic radius. This type of plot is often used to check for systematic trends in diffusive behavior (Hofmann, 1980). Given that the diffusion coefficients of all other major and trace elements show hardly any variation across a broad range of charge and ionic radius, the exceptionally fast diffusivity of lithium is not explained by its charge and ionic radius. We don't yet have a good explanation for why lithium diffuses so fast, but note that two other species, molecular water (Zhang and Stolper, 1991) and helium (Lux, 1987), are similarly fast diffusers in silicate melts.

The demonstration that isotopes can become significantly fractionated by chemical diffusion between natural silicate melts provides a potential fingerprint of mass transport by diffusion. In an earlier paper (Richter et al., 1999), we dis-

cussed how this fingerprint might be used in connection understanding transport between layers in layered intrusions and in igneous cumulates. The most surprising result of our study is the extraordinary mobility of lithium in igneous systems. Lithium is not a commonly measured element in igneous rocks, but our results suggest that lithium might be quite useful in studying local equilibration processes. For example, if one were to find evidence for significant lithium heterogeneity in melts at depth or in erupted lavas it follows that the processes responsible for that heterogeneity (e.g., crystallization, wall-rock contamination, magma mixing, etc.) must have been rapid and active shortly before the magma solidified.

Acknowledgments—We are most grateful for Tom Owens' heroic efforts in measuring the calcium isotopic composition of materials taken from diffusion couples RB-2 and RB-3. This research was supported by Department of Energy Grants to FMR (DE-FG02-01ER15254) and DJD (by the Director of the Office of Energy Research of Basic Energy Sciences, Chemical Sciences, Geosciences and Biosciences Division of the U.S. Department of Energy, under Contract No. DE-AC03-76SF00098 to the E. O. Lawrence Berkeley National

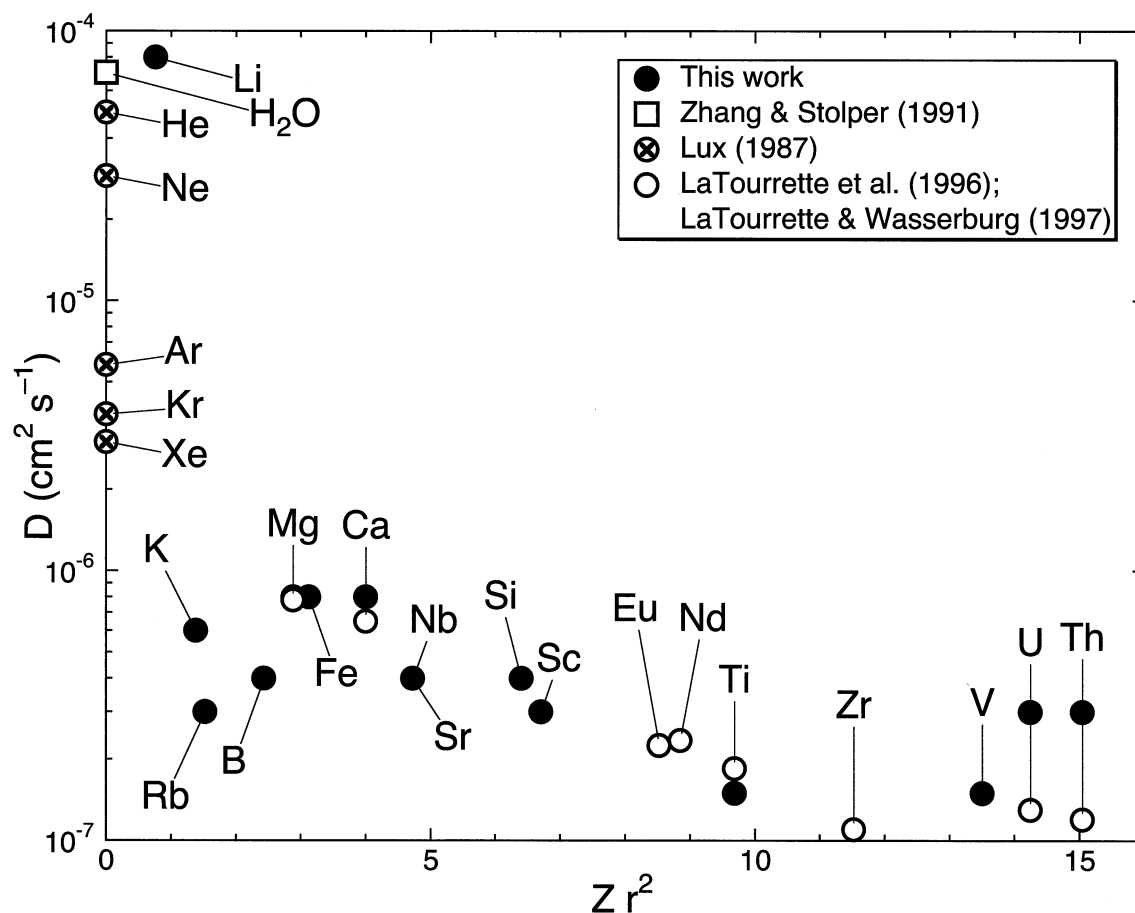


Fig. 12. Diffusion coefficients for lithium and selected trace elements in a basaltic liquid plotted as a function of Zr^2 where Z is the charge and r is the ionic radius. Ionic radii are taken for sixfold coordination from Shannon (1976). Besides our own data, we show for diffusivities for trace elements in a haplobasaltic melt (LaTourrette et al., 1996; LaTourrette and Wasserburg, 1997), for water in a basaltic melt (Zhang and Stolper, 1991), and for noble gases in silicate liquids (Lux, 1987).

Laboratory); a National Science Foundation grant to EBW (EAR-9804794); and a National Aeronautics and Space Administration grant to AMD (NAG5-9510).

Associate editor: F. J. Ryerson

REFERENCES

- Beard B. L. and Johnson C. L. (1999) High precision iron isotope measurements of terrestrial and lunar materials. *Geochim. Cosmochim. Acta* **63**, 1653–1660.
- Chapman S. and Cowling T. G. (1952) *The Mathematical Theory of Non-Uniform Gases*. Cambridge Univ. Press, Cambridge.
- Craig H., Gordon L. I., and Horibe Y. (1963) Isotopic exchange effects in the evaporation of water. *J. Geophys. Res.* **68**, 5079–5087.
- Cooper A. R. (1965) Model for multi-component diffusion. *Phys. Chem. Glasses* **6**, 55–61.
- Davis A. M., Hashimoto A., Clayton R. N., and Mayeda T. K. (1990) Isotope mass fractionation during evaporation of Mg_2SiO_4 . *Nature* **347**, 655–658.
- Davis A. M., MacPherson G. J., Clayton R. N., Mayeda T. K., Sylvester P. J., Grossman L., Hinton R. W., and Laughlin J. R. (1991) Melt solidification and late-stage evaporation in the evolution of a FUN inclusion from the Vigarano C3V chondrite. *Geochim. Cosmochim. Acta* **55**, 621–637.
- Galy A., Belshaw N. S., Halicz L., and O’Nions R. K. (2001) High-precision measurement of magnesium isotopes by multiple-collector inductively coupled plasma mass spectrometry. *Int. J. Mass Spectrom.* **208**, 89–98.
- Hinton R. W., Davis A. M., Scatena-Wachel D. E., Grossman L., and Draus R. J. (1988) A chemical and isotopic study of hibonite-rich refractory inclusions in primitive chondrites. *Geochim. Cosmochim. Acta* **52**, 2573–2598.
- Hofmann A. W. (1980) Diffusion in natural silicate melts: A critical review. In *Physics of Magmatic Process* (ed. R. B. Hargraves). Princeton Univ. Press, Princeton, NJ.
- Humayun M. and Clayton R. N. (1995) Precise determination of the isotopic composition of potassium: application to terrestrial rocks and lunar soils. *Geochim. Cosmochim. Acta* **59**, 2115–2130.
- James R. H. and Palmer M. R. (2000) The lithium isotope composition of international rock standards. *Chem. Geology* **166**, 319–326.
- LaTourrette T. and Wasserburg G. J. (1997) Self diffusion of europium, neodymium, thorium, and uranium in haplobasaltic melt: The effect of oxygen fugacity and the relationship to melt structure. *Geochim. Cosmochim. Acta* **61**, 755–764.
- LaTourrette T., Wasserburg G. J., and Fahey A. J. (1996) Self diffusion of Mg, Ca, Ba, Nd, Yb, Ti, Zr, and U in haplobasaltic melt. *Geochim. Cosmochim. Acta* **60**, 1329–1340.
- Leshner C. E. (1994) Kinetics of Sr and Nd exchange in silicate liquids: Theory, experiments, and applications to uphill diffusion, isotopic

- equilibration, and irreversible mixing of magmas. *J. Geophys. Res.* **99**, 9585–9604.
- Liang Y., Richter F. M., Davis A. M., and Watson E. B. (1996a) Diffusion in silicate melts: I. Self-diffusion in CaO-Al₂O₃-SiO₂ at 1500°C and 1GPa. *Geochim. Cosmochim. Acta* **60**, 4353–4367.
- Liang Y., Richter F. M., and Watson E. B. (1996b) Diffusion in silicate melts: II. Multicomponent diffusion in CaO-Al₂O₃-SiO₂ at 1500°C and 1GPa. *Geochim. Cosmochim. Acta* **60**, 5021–5035.
- Liang Y., Richter F. M., and Chamberlin L. (1997) Diffusion in silicate melts: III. Empirical models for multicomponent diffusion. *Geochim. Cosmochim. Acta* **61**, 5295–5312.
- Lux G. (1987) The behavior of noble gases in silicate liquids: Solution, diffusion, bubbles, and surface effects, with applications to natural samples. *Geochim. Cosmochim. Acta* **51**, 1549–1560.
- MacPherson G. J. and Davis A. M. (1994) Refractory inclusions in the prototypical CM chondrite, Mighei. *Geochim. Cosmochim. Acta* **58**, 5599–5625.
- Marshall B. D. and DePaolo D. J. (1982) Precise age determination and petrogenetic studies using the K-Ca method. *Geochim. Cosmochim. Acta* **46**, 2537–2545.
- Marshall B. D. and DePaolo D. J. (1989) Calcium isotopes in igneous rocks and the origin of granite. *Geochim. Cosmochim. Acta* **53**, 917–922.
- Medford G. A. (1973) Calcium diffusion in a mugearite melt. *Can. J. Earth Sci.* **10**, 394–402.
- Onsager L. (1945) Theories and problems of liquid diffusion. *Ann. New York Acad. Sci.* **46**, 241–265.
- Park R. and Epstein S. (1960) Carbon isotope fractionation during photosynthesis. *Geochim. Cosmochim. Acta* **21**, 110–126.
- Richter F. M., Liang Y., and Davis A. M. (1999) Isotope fractionation by diffusion in molten oxides. *Geochim. Cosmochim. Acta* **63**, 2853–2861.
- Russell W. A., Papanastassiou D. A., and Tombrello T. A. (1978) Ca isotope fractionation on Earth and other solar system materials. *Geochim. Cosmochim. Acta* **42**, 1075–1090.
- Shannon R. D. (1976) Revised effective ionic radii and systematic studies of interatomic distances in halides and chalcogenides. *Acta Crystallogr.* **A32**, 751–762.
- Sherwon P. G. (1963) *Diffusion in Solids*. McGraw-Hill, New York.
- Simon S. B., Grossman L., and Davis A. M. (1991) Fassaite composition trends during crystallization of Allende Type B refractory inclusion melts. *Geochim. Cosmochim. Acta* **55**, 2635–2655.
- Skulan J., DePaolo D. J., and Owen T. L. (1997) Biological control of calcium isotopic fractionation in the global calcium cycle. *Geochim. Cosmochim. Acta* **61**, 2505–2510.
- Tsuchiyama A., Kawamura K., Nakao T., and Uyeda C. (1994) Isotopic effects on diffusion in MgO melt simulated by the molecular dynamics (MD) method and implications for isotopic mass fractionation in magmatic systems. *Geochim. Cosmochim. Acta* **58**, 3013–3021.
- Urey H. C. (1947). The thermodynamic properties of isotopic substances. *J. Chem. Soc.* 562–581.
- Verbeek A. A. and Schreiner G. D. L. (1967) Variations in ³⁹K: ⁴¹K ratio and movement of potassium in a granite-amphibolite contact region. *Geochim. Cosmochim. Acta* **31**, 2125–2133.
- Watson E. B. (1982) Basalt contamination by continental crust: Some experiments and models. *Contrib. Mineral. Petrol.* **80**, 83–87.
- Watson E. B., Wark D. A., Price J. D., and Van Orman J. A. (2002) Mapping the thermal structure of solid-media pressure assemblies. *Contrib. Mineral. Petrol.* **142**, 640–652.
- Zhang Y. and Stolper E. M. (1991) Water diffusion in basaltic melt. *Nature* **351**, 306–309.
- Zhou Y. (1997) Thermodynamic and dynamic properties of multicomponent liquids: A study by molecular dynamics simulation. Ph.D. thesis, University of Chicago.

APPENDIX

The OB series of mixed glass compositions between rhyolitic and basaltic endmembers (Table 2) were synthesized to allow matrix effects on isotopic measurements by ion microprobe to be corrected for. They also permit some interesting tests of matrix effects on ion microprobe measurements of elemental concentration.

All ion microprobe elemental concentration measurements reported in this work assume a single set of calcium-normalized ion yields. Although we don't have independent information on the trace element contents of the endmember rhyolitic and basaltic glasses, we do have such information for major elements from the SEM energy-dispersive X-ray microanalyses. In addition, if ion yields are constant or vary linearly with SiO₂ content, measured concentrations of intermediate composition mixtures should also lie along linear mixing lines between the two endmembers. Major and trace element abundances were measured in each of the OB series glasses, with two to four analyses of each glass. We also calculated the elemental composition of each glass from the measured composition of the endmembers. For the endmembers, we used SEM-EDS analyses for major elements and ion microprobe analyses for trace elements. We then normalized the measured concentrations for all glasses to these interpolated values (Fig. A1). Trace elements have normalized values of one at each end, by definition.

Considering the major elements first, the ion microprobe analyses are within 20% of true values in all cases. There appears to be a steady increase in ion yield of Na with SiO₂ content, and a slight decrease in that of Ti. Fe shows a pronounced dip at ~70 wt.% SiO₂, indicating that ion yield for this element is not a smooth function of composition.

For the trace elements, several of the intermediate glasses appear to have been contaminated with selected elements. All replicate analyses of these glasses showed the same effect, so there is a bulk contamination of the glass, not a surface contamination. Sample OB-7, the first one from the basaltic end, is clearly enriched in chromium, lanthanum and neodymium (Fig. A1). The fact that these enrichments are not seen in cerium and praseodymium strongly suggests laboratory contamination. Fortunately, contamination of glass is not widespread and there are enough intermediate glasses that it can be easily recognized.

The trace elements have curves in Fig. A1 that fall into characteristic groups for chemically similar elements. Disregarding the two chromium-contaminated glasses, the curves for the transition elements chromium, manganese and iron are remarkably similar. The rare earth elements, as well as thorium and uranium tend to show positive deviations at intermediate values. Vanadium, a high-charge transition element shows a similar effect. The light elements lithium and beryllium tend to show negative deviations at 55–60 wt.% SiO₂. Of the remaining trace elements, beryllium, scandium, rubidium, strontium, yttrium, niobium, zirconium, barium and europium are remarkably flat and well-behaved.

In conclusion, ignoring matrix effects in the ion yields of trace elements gives results that are within 20 relative % of interpolated values. Given that the trace element concentration gradients for most elements are factors of 5 to nearly 100 in the experiments reported here, uncertainties in trace element concentrations have little effect on inferred diffusion coefficients.

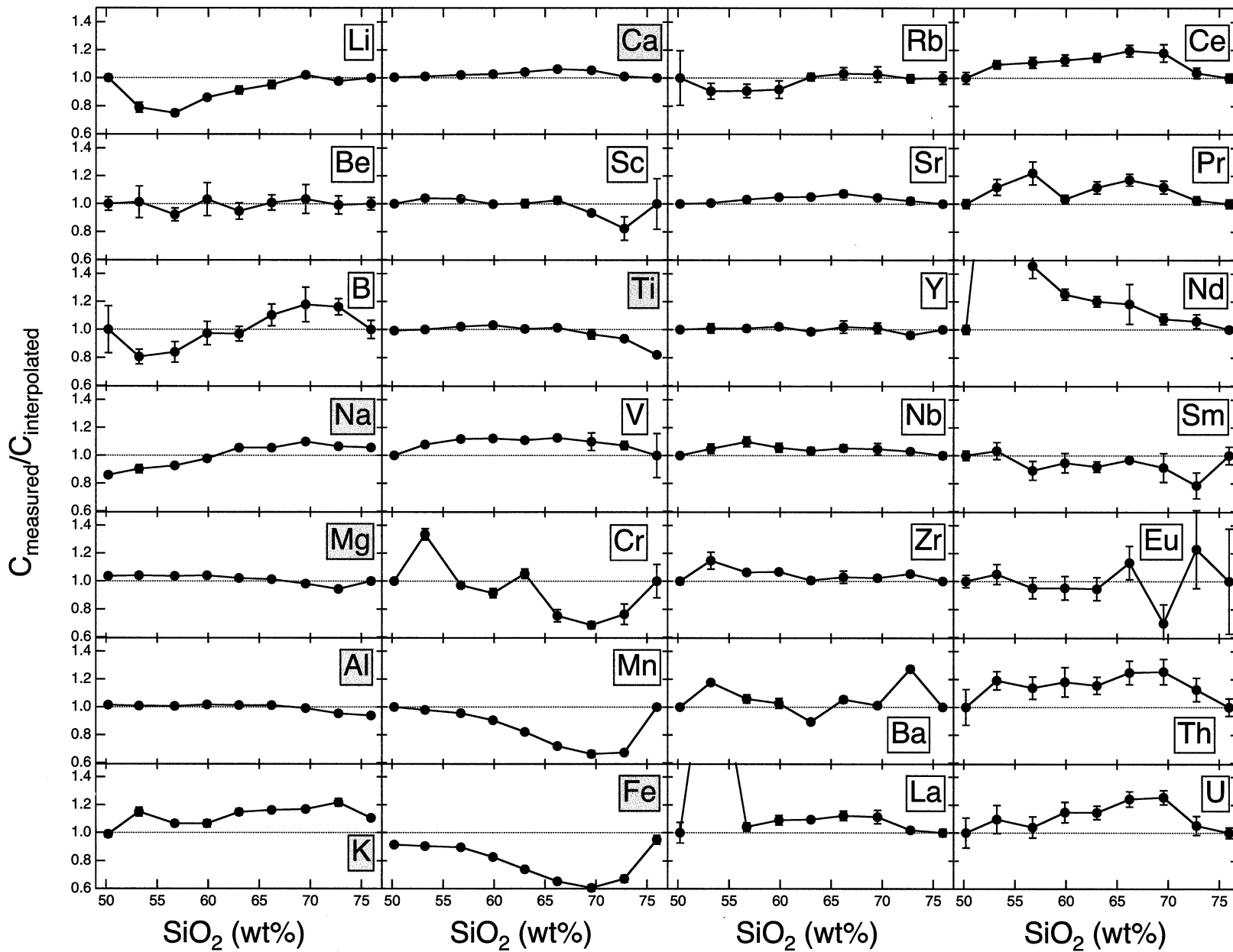


Fig. A1. Concentrations in the OB series samples of mixed rhyolite-basalt compositions, measured by ion microprobe and normalized to values calculated by linear interpolation between endmember basalt and rhyolite. Shaded labels indicate elements for which endmember compositions were determined independently by EDS. For all elements, endmember normalized concentrations are 1, by definition.